3-1-1991

Threshold modulation in 1-D error diffusion

Katrien Daels

THRESHOLD MODULATION IN 1-D ERROR DIFFUSION

By

Katrien Daels

March 1991

A THESIS SUBMITTED IN PARTIAL FULFILLMENT

OF THE REQUIREMENTS FOR THE DEGREE OF

MASTER OF SCIENCE IN THE CENTER FOR

IMAGING SCIENCE IN THE COLLEGE OF

GRAPHIC ARTS AND PHOTOGRAPHY OF THE

ROCHESTER INSTITUTE OF TECHNOLOGY

Signature of Author

Katrien Daels

Accepted by

Name Illegible

Coordinator, M.S. Degree Program

COLLEGE OF GRAPHIC ARTS AND PHOTOGRAPHY

ROCHESTER INSTITUTE OF TECHNOLOGY

ROCHESTER, NY

Certificate of Approval

M.S. DEGREE THESIS

I certify that I have read this thesis and that in my opinion it is fully adequate, in scope and in quality, as satisfactory for the thesis requirements for the Master of Science degree.

Dr. Reiner Eschbach
Webster Research Center
Xerox Corporation

Dr. Roger L. Easton
Center for Imaging Science
Rochester Institute of Technology

Dr. Peter G. Anderson
Computer Science Department
Rochester Institute of Technology

May 16, 1991
Date

THESIS RELEASE PERMISSION FORM

ROCHESTER INSTITUTE OF TECHNOLOGY

COLLEGE OF GRAPHICS ARTS AND PHOTOGRAPHY

I, Katrien Daels, prefer to be contacted each time
a request for reproduction is made.

116 Pebble Beach Rd

Lakeville NY 14480

Date: may 10 1991

Signature: _____

THRESHOLD MODULATION IN 1-D ERROR DIFFUSION

By

Katrien Daels

SUBMITTED TO THE

CENTER FOR IMAGING SCIENCE

IN PARTIAL FULFILLMENT OF THE REQUIREMENTS

FOR THE MASTER OF SCIENCE DEGREE

AT THE ROCHESTER INSTITUTE OF TECHNOLOGY

Abstract

Error diffusion (ED) is widely used in digital imaging as a binarization process which preserves fine detail and results in pleasant images. The process resembles the human visual system in that it exhibits an intrinsic edge enhancement. An additional extrinsic edge enhancement can be controlled by varying the threshold. None of these characteristics has yet been fully explained due to the lack of a suitable mathematical model of the algorithm. The extrinsic sharpening introduced in 1-D error diffusion is the subject of this thesis. An available pulse density modulation(PDM) model generated from a frequency modulation is used to gain a better understanding of variables in ED. As a result, threshold variation fits the model as an additional phase modulation. Equivalent images are obtained by applying ED with threshold modulation or by preprocessing an image with an appropriate convolution mask and subsequently running standard ED.

Acknowledgements

I would like to express my sincere thanks to my advisor, Reiner Eschbach for his guidance, support and patience throughout the work related to this thesis. I am also grateful to the other members of Xerox WRC for helping with hard- and software problems: especially thanks to Rob Rollestone, Bill Fuss, Judith Stinehour and the "trailer"-people. Thanks to Eran, with whom it has been a pleasure to work.

Thanks to Roger Easton who spend a lot of time in *Americanizing* the initial version of this work, and thanks to Peter Anderson for volunteering to be a third advisor.

Special thanks to my husband Geert for his patience and support.

I gratefully acknowledge the financial support I have received from Xerox Corporation through RIT.

Contents

List of Figures

Introduction

Halftoning refers to any technique that converts continuous-tone images into bitonal images while still giving the impression of graytone. This is obviously important for printing images. The most common application of rendering photos into binary elements dates back to 1852, when the photomechanical invention of W.H. Fox Talbot[Tal52] was patented and titled "Improvements in the Art of Engraving". The original image is photographed through a so-called halftone screen which multiplies a non-image related light distribution with the exposed image. After photographic processing for high contrast the image achieved has only black and white levels but may represent the original reasonably.

Nowadays halftoning describes a process of converting a digital N-bit image into an image quantized to a single bit. This is essential for displaying images on binary output devices, *e.g.*, a binary video, single-ink printing *etc.* The problem sketched above is very general and may be described as: compression of a two-dimensional signal of N-bit dynamic range into a binary signal. Compression generally refers to methods for reducing the number of bits without loss of full information which is mathematically defined as the negative logarithm of the probability. The decrease in dynamic range from 8 bits to 1 bit generally implies a reduction in image information. The halftoning process may be described as a decision of what data to eliminate,or how to reduce the number of bits without significant loss of image quality as perceived by a human observer. Therefore

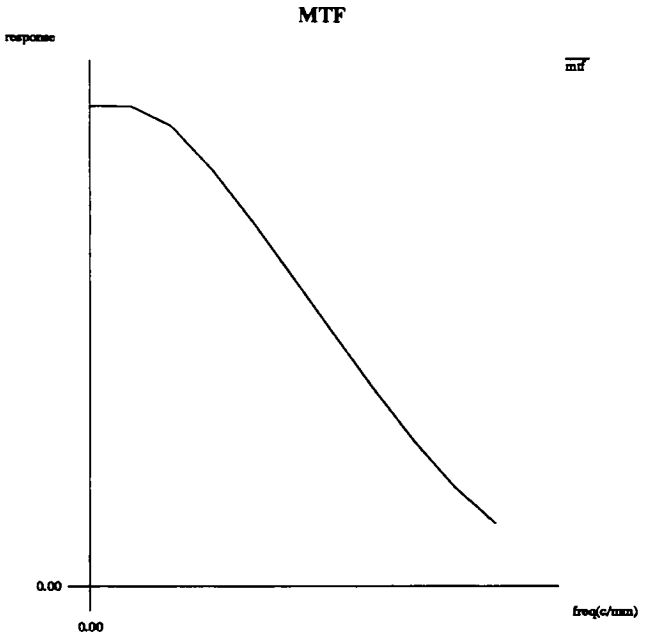

Figure 0.1: Modulation Transfer function of the eye

only that information to which the human visual system is sensitive will influence the critical judgement of the observer of the quality of the binary image. The modulation transfer function of the eye (Fig.0.1) is seen as the ultimate bandpass filter of the imaging system; spectral components outside the passband are not visible. Within the range of frequencies to which the eye is sensitive, low frequencies are detected much better than higher frequencies. After translating this relationship into quality estimates, it can be stated that fine detail becomes more difficult to detect or that the number of discernable gray levels diminishes as the visual angle of the image detail decreases. These limitations of the human visual system are eagerly exploited when developing halftoning algorithms. A strong interest in the problem of halftoning is also shown by the color industry, which applies the binarization technique on the different color channels.

Although the problem of halftoning was originally restricted to binarization methods, there is also significant interest in algorithms which can easily be extended to reduce the dynamic range of the output image to an arbitrary number of bits $M < N$. There would

be more freedom to optimize the output for matching to the characteristics of the human visual system.

Another application of halftoning is to construct a computer generated hologram (CGH), which is a Fourier or Fresnel transformation of the image it will reconstruct. Computer generated holograms must often be binarized for display. The error of the binarization is usually spread in Fourier domain. Error diffusion seems to be a particularly valid method since the noise it creates may appear as localized clouds in the reconstruction of the CGH if the parameters are well chosen. By localizing the image outside the noise cloud, the quality of the reconstruction may be significantly improved.

By its optimization and subsequent broadening of its field of application, halftoning has become a research topic with contributions from several scientific backgrounds, including optics, psychophysics, information theory, computer science, statistics, color science and opto-electronics.

Besides its ability to render high-frequency content, the success of ED is partially due to its inherent edge enhancement [Kno89] which well matches the non linear response of the eye as demonstrated by the psychovisual experiments of Cornsweet [Cor70]. In addition to the intrinsic edge enhancement, a controllable extrinsic edge enhancement has been obtained by varying the threshold in ED [EK91]. Both phenomena have yet to be satisfactory explained.

Chapter 1 provides an overview of halftoning techniques and particularly considers three groups of algorithms: ordered dither, error correction and iterative methods. In Chapter 2, we will elaborate on the error diffusion method of Floyd and Steinberg [FS76], for two reasons. First, the quality of the results obtained from error diffusion exceeds that of any of the dither screens, and its simplicity is very attractive when compared to computationally intensive iterative methods. Moreover, the generalization of error

diffusion to M-bit coding is straightforward. Secondly, there are still some fundamental, intriguing questions, to be answered about error diffusion. The pulse density modulation will be investigated as a model for one- dimensional ED in chapter 3, and will be used to model the extrinsic edge enhancement in ED in chapter 4. In chapter 5, the insight in threshold modulation developed in previous chapter by the comparison to 1-D ED will be used to investigate some characteristics of the results obtained by varying the threshold in two dimensions.

Chapter 1

Binarization Processes

The essential part of each method of binarization consists of a clipping process. Clipping compares the input to a locally stationary threshold, and generates a binary output (0 or 1) according to the sign of the result. This operation is highly non-linear and the analytical description of the binarization process is complicated. The image resulting from it is familiar from advertising and label type images. Contrast will be increased only for values near threshold level, where an artificial separation of gray levels generates contours, which do not necessarily correspond to sharp edges in the image and are therefore called pseudo-contours. As the threshold is varied, these pseudo-contours will move to places with the corresponding intensity value in the image. Figures (1.1,1.2) show the result of clipping the same 8-bit input image with range $[0, 255]$ at different threshold levels. No information of intensity variation above or below threshold is maintained, nor is there any visible effect of gray tone reproduction. The technique is often applied to stylize the image content in advertising. Other binarization methods attempt to refine the clipping process in order to introduce the illusion of gray value when observing the results, and to increase detail reproduction. Also, the visibility of pseudo contours needs to be reduced. According

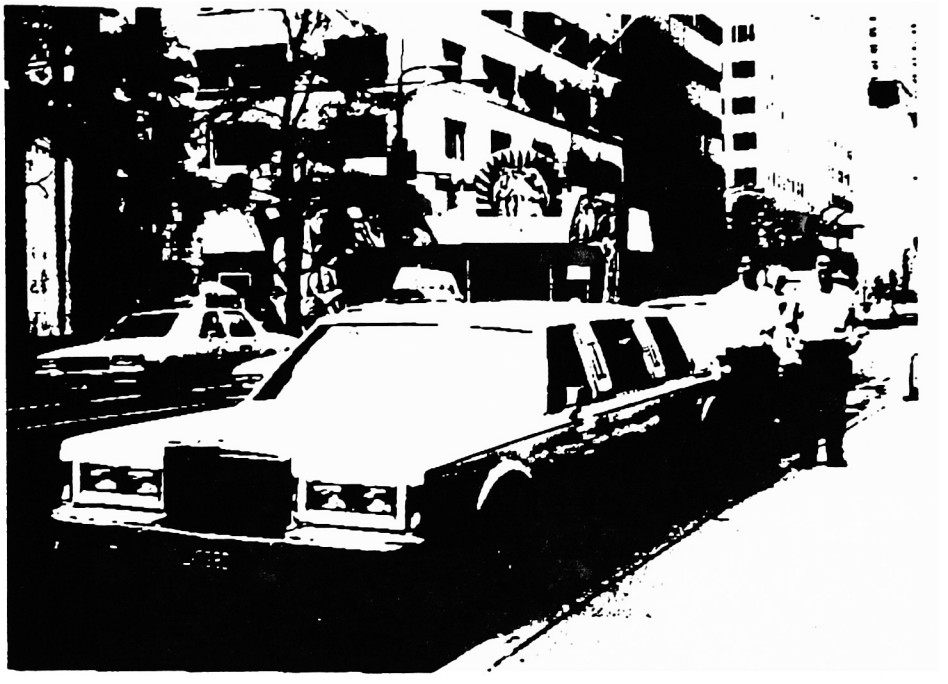

Figure 1.1: Clipped image at threshold = 100

Figure 1.2: Clipped image at threshold = 200

to the response of the eye, the first interest of perceiving gray levels will be most important in the low frequency region, *i.e.* in very smooth areas of the image. The only possible way to create the impression of gray with black and white intensities is to make use of the limited resolution of the human eye and its low pass characteristic. The reproduction of fine detail depends on how well high frequencies are reproduced. It is known that the response of the eye is non linear and will emphasize edges. This is due to lateral inhibition of the retinal receptors and results in highpass. If artifacts occur, they should be of the type of which the eye is not very sensitive. In this section three different types of binarization will be distinguished.

1.1 Locally stationary thresholding

Locally stationary thresholding describes a class of methods that is restricted to adapting the clipping process only by changing the threshold in a predetermined way, generally independent of the input.

Many of these algorithms can be classified as examples of *ordered dithering*, which is completely characterized by the so-called halftone screen. While this screen may correspond to a physical screen consisting of transparent glass in the photomechanical process of Talbot, it can also be defined as a two-dimensional grid of numbers indicating the local clipping levels for electronic screening. Both structures can be characterized by a unit cell of dimension MxN, which after translation covers the whole grid without overlap. Within the unit cell, the amplitude values of the thresholds t(m,n), with $0 \leq m \leq M-1$ and $0 \leq n \leq N-1$ are distributed uniformly between 0 and 1 (after normalization of the input), to give MN + 1 levels of gray over an M x N region. The process of halftoning is obtained for an input function f(i, j) by comparing it to the periodical threshold function as follows:

$$output(i,j) = \begin{cases} 1 & \text{if } f(i,j) \geq t(i \bmod M, j \bmod N) \\ 0 & \text{otherwise.} \end{cases}$$

The threshold unit cell is often referred to as the *threshold profile* or *dot profile*. For a constant input level I_1 the number of thresholds exceeded will be proportional to I_1 and therefore the gray value integrated over one cell will be conserved. Limb[Lim69] proposed this ordered dither for displaying images on a quantized level monitor, while Lippel and Kurland[LK71] applied the idea to binarize continuous tone pictures.

A lot of effort has been spent to optimize the dot profiles. The theoretical limits for optimizing the binarization process for visual output (Fig. 1.3) was described by Roetling[Roe76b] and indicated that halftoning has the possibility to approximate the

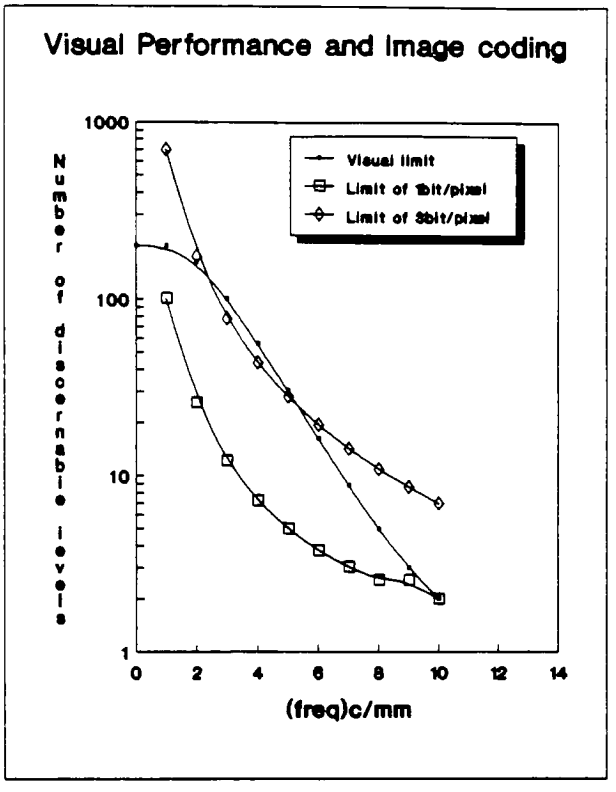

Figure 1.3: Code Limits in spectral domain [Roe76b]

human visual system in the distribution of reproducible levels as function of spatial frequency. The modulation transfer function for a binary image representation on a grid of sample interval $\triangle$ has been obtained by calculating the number of levels L_{f_s} which will respond to a frequency f_s:

$$L_{f_s} = \frac{1}{(2f_s\triangle)^2} + 1 \tag{1.1}$$

and in general for m bits:

$$L_{f_s} = \frac{2^m - 1}{(2f_s\triangle)^2} + 1 \tag{1.2}$$

This MTF respects the drop off of the sensitivity toward distinguishing gray levels with increasing frequency. However in the case of ordered dither, there is an inevitable trade off between the maximum number of gray levelsL_0 at zero frequency and the maximum frequency reproducible in x and y direction (F_x, F_y), both depending on the size of the

dither screen:

$$L_0 = MN \tag{1.3}$$

$$F_x \sim \frac{1}{M} \tag{1.4}$$

$$F_y \sim \frac{1}{N} \tag{1.5}$$

$$\tag{1.6}$$

The resolution of the device determines more or less the size of the mask to guarantee that the eye averages the pixels over one screen cycle at normal viewing distance. Equations (1.3,1.4,1.5) show the interdependency of the number of gray levels and the halftone frequency. This coupling represents an inherent trade-off for the ordered dither schemes, trying to minimize the visibility of the halftone screen while simultaneously producing sufficient gray level resolution so that the observer does not perceive quantization contouring. Depending on the arrangement of the threshold levels, certain spatial frequencies will be favored and thus the binarized image will exhibit specific screen-related texture.

Bayer[Bay73] optimized a dot pattern so that the amplitude of longest finite wavelength of the non-zero sinusoidal component of the dot pattern is minimal. In this way the most visible texture is diminished. For an 8×8 screen the optimization requires that 32 threshold levels be symmetrically positioned around the center as in Fig.(1.4). The result is a dot profile in which the sequential threshold values, T_1 and $(T_1 + 1)$ are spatially located as far as possible away from one another [Stu75]. Bryngdahl [Bry78] formulated the requirements of optimal detail rendition in terms of the shape variations of the dot peripheries without making calculations in frequency domain. Image information in the case of clipping is only given when the image intensities cross the threshold surface (Figure (1.5)). The more often this happens, the more information will be contained in the

0	16	4	20	1	17	5	21
24	8	28	12	25	9	29	13
6	22	2	18	7	23	3	19
30	14	26	10	31	15	27	11
1	17	5	21	0	16	4	20
25	9	29	13	24	8	28	12
7	23	3	19	6	22	2	18
31	15	27	11	30	14	26	10

Figure 1.4: Threshold profile of Bayer's screen

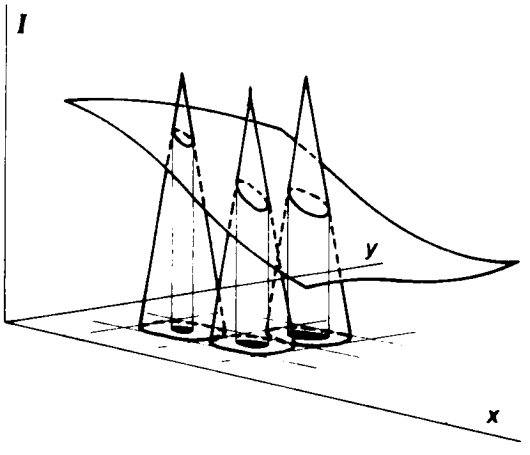

Figure 1.5: Representation of clipping the image content with concentric dot profiles, (Figure taken from [Bry78])

11	0	15	7	4	11	4	7	15	0
2	9	12	19	16	22	18	21	14	8
15	14	24	3	6	10	5	1	24	12
7	21	1	13	20	23	17	13	3	19
4	18	5	17	8	0	9	20	6	16
11	22	10	23	2	11	2	23	10	22
4	16	6	20	9	0	8	17	5	18
7	19	3	13	17	23	20	13	1	21
15	12	24	1	5	10	6	3	24	14
2	8	14	21	18	22	16	19	12	9

Figure 1.6: Threshold profile of Bryngdahl's screen

binary output image. Expressed differently, the information is exclusively present in the zerocrossings of the output image, when the two binary output values are set symmetrically around 0 (*e.g.*$-1, +1$). This reasoning resulted in a threshold function with a halftone geometry consisting of two concentric rings. For a 10×10 screen this results in Fig (1.6)

The result of these dither masks can be evaluated in Figures(1.7,1.8). Both of these patterns optimize the screen for a specific formulated optimum concerning spatial resolution, generating *dispersed dot patterns*. The fact that the final dot is dispersed is usually a disadvantage when using real output devices. The area covered by one sample dot used in printing is mostly circular and often overlaps neighboring dots, versus the theoretical squared area.

The merit of the *clustered dot patterns* is that loss in tonal fidelity due to the non-ideal area coverage is reduced when the activated samples in one period of a halftone screen exhibit a minimal perimeter. By using tonal-fidelity rendition as the first criterion for optimization, the resulting threshold profile positions the threshold values T_1 and $(T_1 + 1)$ as close to each other as possible. The second criterion which shapes the dots along the 45° and 135° diagonals, is essentially the same as used by Bayer; it considers the decreased

Figure 1.7: 5th avenue, processed by Bayer's screen

Figure 1.8: 5th avenue, processed by Bryngdahl's screen with concentric ring symmetry

Figure 1.9: 5th avenue,processed by the clustered dot screen

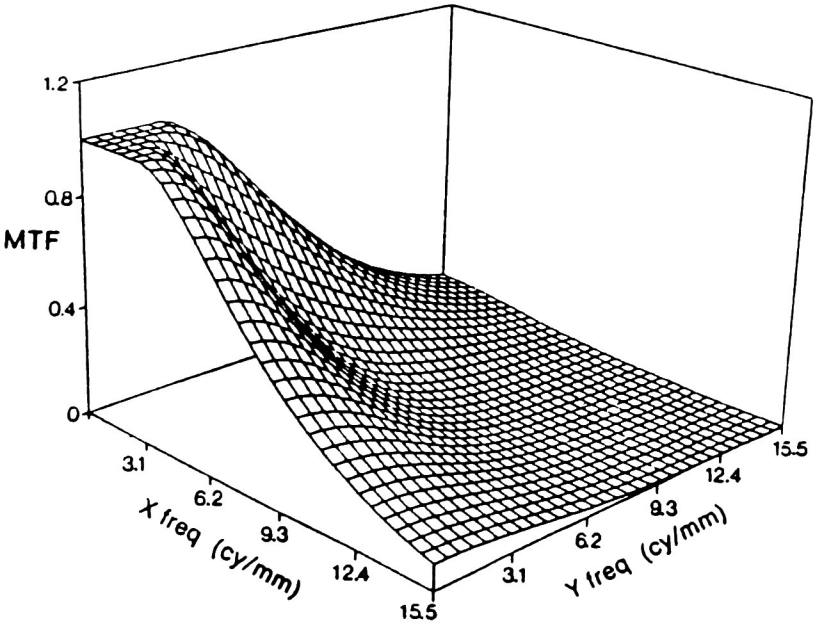

Figure 1.10: 1 quadrant of the visual transfer function, (Figure taken from [SM90])

19	25	23	17	14	8	10	16
21	31	29	27	12	2	4	6
28	30	32	22	5	3	1	11
18	24	26	20	15	9	7	13
14	8	10	16	19	25	23	17
12	2	4	6	21	31	29	27
5	3	1	11	28	30	32	22
15	9	7	13	18	24	26	20

Figure 1.11: Threshold profile of a clustered dot

sensitivity of the eye in these directions (Fig. 1.10) and allows the longest wavelengths responsible for texture to have these orientations. An example for a screen with clustered dot is given in Fig.(1.11), and the result of applying the mask on the test image is shown in Fig.(1.9).

T. Holladay[Hol80] described a compact way of creating halftone dotprofiles for arbitrary angles of the screens.

Study of the Fourier spectrum[KR75] proves that image detail is maintained at spatial frequencies greater than half of the screen frequency. Moiré patterns may occur depending upon object contrast and the halftone dot pattern. Moiré patterns may be reduced by making the dot patterns quasi periodic[AL76]. This controlled type of randomization introduces noise only at higher diffraction orders of the spectrum of the halftone image. However, the overall appearance is noisy. Some explanation can be found in the fact that the noisy threshold has a flat power spectrum, while the visual system has a bandpass character.

Jarvis and Roberts[JR76] proposed a method in 1976 to adapt the threshold in the clipping process to be linearly dependent on the local average of neighboring pixel values, and called the process constrained average algorithm. Because the averaging operation can be considered as a stationary operation described by its filter values, the thresholding

executed will be locally stationary and hence the classification of this algorithm is justified. If $I_{av}(x, y)$ is the local average at pixel (x, y), the threshold is determined by

$$T(x, y) = \gamma + (1 - \frac{2\gamma}{I_0})I_{av}(x, y) \tag{1.7}$$

where γ is a parameter controling the variability of the threshold around I_0, also determining the amount of contrast in the resulting binary image. It is easily seen that $T(x, y)$ ends up in the interval $[\gamma, I_0 - \gamma]$. For $\gamma = 0$, the threshold equals the local average, resolving detail that deviates from the average gray level. For $\gamma \neq 0$ contrast will increase. A similar dynamic thresholding was proposed by Morrin[Mor74], but the input is subjected to the dynamic thresholding only when its value lies in the midrange between two predetermined threshold values $[A_{min}, A_{max}]$. This assures that extremes turn on to the corresponding closest binary representation.

1.2 Error correction methods or globally adaptive thresholding

Error correction methods modify the input before clipping. This modified input is obtained by comparing input and binary output in order to minimize a predefined error. The threshold and/or input is changed based on image content or previously processed values and is not known in advance.

Roetling introduced the ARIES [Roe76a] method, which stands for *Alias Reducing Image Enhancing Screener*. The output is guaranteed to have the minimum deviation of the average input reflectance over one halftone cell. This is done by adapting the ordered dither algorithm by adjusting the threshold level of ordered dither in each halftone cycle. A normal halftone screen preserves the average gray level only in constant regions; moiré patterns or aliasing can occur in regions of the image that contain high spatial frequencies. Because ARIES adjusts the average gray scale for each halftone cycle, the low frequencies of the image are preserved and aliased low frequency (which usually span several halftone cells) will be reduced. A certain edge enhancement is obtained at both low and high contrast edges. The clustered dot threshold profile in combination with ARIES results in Figure 1.12. Manfred Schroeder [Sch69] described a series of algorithms which try to compensate for previously made errors between output and input values. The intensity of the original picture $I(x, y)$ should be obtained by lowpass filtering the current output. A modified input $\acute{I}(x, y)$ at point (x,y) is generated to compensate for the error E(x, y):

$$E(x, y) = I(x, y) - B(x, y) \tag{1.8}$$

between input I and output B made earlier in a predefined neighborhood (Figure 1.14).

Figure 1.12: ARIES applied on clustered dot

Figure 1.13: Regular screening with clustered dot

This modified input

$$\acute{I}(x,y) = I(x,y) + (1/\sum_{i,j} \alpha_{ij}) \sum_{i,j} \alpha_{ij} E(x+i, y+j) \tag{1.9}$$

is the original input combined with a lowpass version (α_{ij}) of neighboring errors, and will be submitted to the standard clipping process with fixed threshold $T = \frac{I_0}{2}$. The transfer of the errors is illustrated in Figure (1.14), while the result of the algorithm is shown in Figure (1.16). Depending on the size of the averaging mask, the algorithm requires line memories to store the calculated errors for further processing. It is obvious that this type of algorithm is restricted for use in digital processing and has no equivalent in photographic techniques. Hale [Hal76] proposed Dot Spacing Modulation (DSM), which is the digitized version of an analog frequency modulation method described by Klensch [KMW70] and its time sampled version described by Inose [IY62]. During the one-dimensional scanning of the digital image, the sampled values are added into a storage register $S = \sum_{j=1}^{n} I_j$. As soon as the total number in the storage register exceeds a predefined threshold T, the output is set to "1" and the remainder

$$R = \sum_{j=1}^{n} I_j \bmod T \tag{1.10}$$

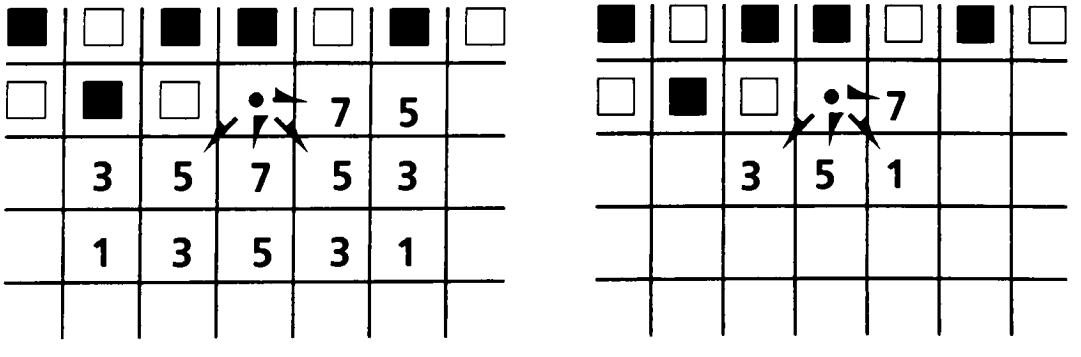

Figure 1.14: Distribution of error in Schroeder's and Floyd's algorithms

Figure 1.15: 5th, avenue processed by standard error diffusion

Figure 1.16: Schroeder's error correction with original weights

is part of the next sum in the store register

$$S = \sum_{j=1}^{n} I_j \bmod T + \sum_{j=n+1}^{m} I_j. \tag{1.11}$$

Vertical detail is nicely reproduced, while horizontal detail is rendered less sharply. This preference of direction is easily understood, as the DSM is a one-dimensional algorithm.

At about the same time, Robert W. Floyd and Louis Steinberg [FS76] presented their two-dimensional error diffusion method. The algorithm transfers errors to unprocessed pixels in several directions and the resulting modified input level is compared to a fixed clipping level. The algorithm is applied sequentially, while scanning the image line by line from left to right. The error transferred from the pixel at position (i, j) = (column, row) will be distributed to pixel $(i+1, j), (i+1, j+1), (i, j+1), (i, j-1)$, with respective weights $\frac{7}{16}, \frac{1}{16}, \frac{5}{16}, \frac{3}{16}$. Note, the sum of the weights is unity. The error is the difference between the binary output gray level and the modified input level. This method preserves the overall integrated gray level, and is able to reproduce fine detail in both horizontal and vertical directions as illustrated in Figure (1.15).

The error diffusion algorithm differs from Schroeder's algorithm only in the error calculation. Schroeder's definition of the error the difference between the output level and the original, not the modified, input level. Therefore he did not obtain a correct integrated gray level. Compared to the dithered results in Figures (1.7, 1.8, 1.9), both error correction methods show superior edge rendition. ED also exceeds the other methods in overall image representation.

The disadvantages of ED include visible textural or wormlike defects and complex computation compared to ordered dither. Several attempts have been made to adapt the error diffusion algorithm solve these problems. A method for faster computation without too many adaptations has been suggested by Kurosawa [KMNK89] by requiring that the reciprocal of the weights be integral powers of two.

Knuth [Knu87] proposed a dot diffusion algorithm which tries to combine the positive aspects of both ED and ordered dither. The idea of distributing the error is present, together with a clustered dot screen. The screen classifies the pixels into a hierarchic system that indicates the order of processing; pixels near the top of the hierarchy are processed first. The errors are distributed only to neighbors with lower hierarchic position, which means they are yet to be processed. The distribution of the error ensures that details are nicely reproduced, but areas of near constant gray level are disturbed by a grain-like texture. To reduce the visibility of the texture, small variations in the threshold were introduced about the original fixed value of $\frac{I_0}{2}$. This idea originates from Billotet-Hoffmann and Bryngdahl [BHB83], which discovered a pleasant improvement when applied in error diffusion.

Stucki [Stu81] proposes a Multiple-Error Correction Computation Algorithm called MECCA. It is another attempt to improve classical ordered dither by incorporating some error diffusion. The purpose is to generate pseudo-disordered dot patterns and to correct for non-ideal printing. Depending on the weights and the extension of the distribution, some orientations in the spectrum might be favored and result in edge enhancement. A look-ahead filter is used to compensate for the non-ideal response of the error diffusion algorithm, before the image is processed. After the adapted error diffusion is calculated, a second error diffusion is executed on this output in order to compensate for dot overlap by the non-ideal printing device.

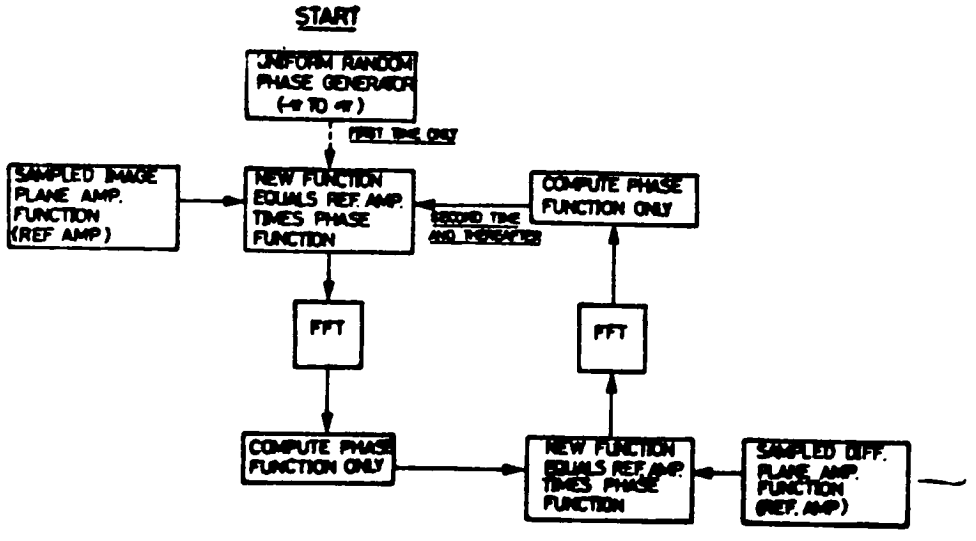

Figure 1.17: Iteration by Gerchberg and Saxton (Figure taken from [GS73])

1.3 Iterative methods

Iterative methods use aspects of both previously mentioned groups, but can be distinguished easily because the binarization decision needs several global iterations. Several algorithms come from different applications. It is obvious that the direct implementation of iterative algorithms is more difficult and might be limited by computation time. However their construction is often based on more rigorous theoretical grounds and the understanding of the principles involved can lead to simpler non-iterative approaches.

A series of algorithms is based on a recursion scheme designed by R. W. Gerchberg and W.O. Saxton [GS73] who presented it as a way to determine the phase of a wave function when its intensity is known both in the diffraction and imaging plane. It iterates between a function and its transformation (*e.g.* Fourier), where constraints are applied alternately in function and transform domains. The outline is sketched in Figure(1.17). The initial distribution of the phase is arbitrary and is usually assumed to be uniformly random. This phase is combined with the amplitude calculated from the intensity in the

image plane to form a complex function which will be transformed to the other domain in each cycle. In each step the phase distribution is maintained, while the amplitude function is recalculated based on the constraints of the known intensities in the image and diffraction planes. The intermediate result varies as long as the phase function is modified by the transformation. Absolute convergence to the correct complex amplitude cannot be proven but the algorithm guarantees that the error cannot increase, where the error is defined as the sum of the squared differences between the amplitudes of the actual and calculated data in either domain.

Broja, Wyrowski and Bryngdahl [BWB89] applied this principle to binarize continuous-tone images by matching the constraints of the iterations to the specific needs of binarization. Their constraint in the space domain is the restriction to a binary output, while that in the Fourier domain is a lowpass filter. To avoid a quick stagnation of the recursion, the space-domain binarization is introduced stepwise by using a threshold based on a parameter g_j, which lies in the range $g_j \in [0, 0.5]$ and which increases with increasing number j of iteration cycles:

$$\begin{aligned} B_j(I) &= 1;\ for\ I \geq 1 - g_j \\ &= I;\ for\ g_j \leq I \leq 1 - g_j \\ &= 0;\ for\ I < g_j \end{aligned} \tag{1.12}$$

The binarization noise introduced by the soft clipping is gradually pushed out of the lowpass region to higher frequencies where it is less noticeable to the eye.

A more straightforward iterative approach searches the space of binary images for the one that minimizes the measure of error chosen. For a 256×256 image this space contains $2^{256 \times 256}$ elements. The direct binary search (DBS) [SAS87] was used to optimize binary

computer generated holograms for which the desired intensity of the Fourier transform is known. The search starts with a uniformly random binary image for which an error function is defined. Each pixel is examined to decide whether switching the binary output would reduce the error function value. If so, the switch is accepted and the next pixel is treated; if not, the original value is retained. This search is a regular minimization problem which follows the negative gradient on the error surface and stops at a local minimum. The inclination of the error surface determines the velocity of the convergence and the initial starting point determines which local minimum is achieved. Obviously, the global minimum of the error surface is the best result and this method will not necessarily reach it. By introducing more freedom on the path taken on the error surface the likelihood of reaching the global minimum may be increased. The simulated annealing technique [GG84], is one method that was adapted from the principle of solid-state physics. The individual output pixels can be viewed as atoms or molecules in a lattice-like physical system with two possible energy states, *e.g.* molecules with a spin = $\frac{1}{2}$ in the presence of a magnetic field. The energy state of the lattice is non-deterministic but may be described by a probability given by its Gibbs distribution:

$$P(U_j) = \frac{e^{-\beta U_j}}{\sum_j e^{-\beta U_j}} \tag{1.13}$$

where U_j the energy state of the whole image, and $\beta = (kT)^{-1}$ is a temperature factor which specifies the entropy. While the direct binary search allowed only state changes with lower energy, simulated annealing allows the transitions to higher energy with a certain probability equal to the Gibbs factor. By gradually reducing the temperature of the whole system, the system is slowly forced to isolated low energy states ("annealing"), which are the most probable states under the Gibbs distribution. For simulated annealing to be successful, it is important to find a good model for the energy of the image. The case where $T = 0$ reduces simulated annealing to the gradient method of DBS.

Another iterative method related to relaxation is the model of Eschbach and Hauck [EH87a], which defines a potential field due to nearest-neighbor interaction. The amplitude of the force (= derivative of the potential field) is inversely proportional to the square of the distance between pixels. The proportionality constant is determined by the inverse of the squared intensity level between the pixels involved. The vectorial description for the force is :

$$\vec{F_{ij}} = \vec{e_{ij}} \frac{F_0 D_0^2}{I_{ij} D_{ij}^2}, \tag{1.14}$$

with $\vec{e_{ij}}$ a directional unit vector on the line connecting pixels i,j and F_0 is a constant. Because of the unability to escape from local minima (= zero temperature condition in simulated annealing) an appropriate starting position is required to obtain a satisfactory output.

Chapter 2

Error Diffusion:

Appearance and Approaches

Error diffusion has been shown to give superior results when compared to other binarization methods (section 1). The detail rendition is rendered very well as can be seen in Figure(1.15), and the overall result is very pleasing to the eye. However, error diffusion also exhibits some annoying artifacts which are most visible in slowly varying regions of the image and thus provide a challenge to search for the optimized version.

2.1 Definition

The error diffusion technique as originally introduced by Floyd and Steinberg [FS76] modifies the intensity I at pixel x and column y to $\tilde{I}(x,y)$ by distributing previously computed errors :

$$\tilde{I}(x,y) = I(x,y)+aE(x-1,y)+bE(x-1,y-1)+cE(x,y-1)+dE(x+1,y-1). \quad (2.1)$$

The error E(x, y), diffused by the four neighboring positions which are already processed, is the difference between the modified input and the resulting binary output:

$$E(x,y) = \tilde{I}(x,y) - step(\tilde{I}(x,y) - T), \tag{2.2}$$

where T is the fixed threshold used to hardclip the adapted input in order to binarize the output:

$$B(x,y) = step(\tilde{I}(x,y) - T). \tag{2.3}$$

The weights a, b, c, d were defined so as to obtain a checkerboard pattern when the input is midgray, for $I = \frac{I_{max}}{2}$. The respective weights are $\frac{7}{16}, \frac{1}{16}, \frac{5}{16}, \frac{3}{16}$.

2.2 Artifacts in ED

The artifacts appearing in error diffusion has been a topic of extensive study. In a textbook based on a doctoral thesis by Ulichney [Uli87] three types of artifacts in halftoning are defined:

- correlated artifacts in certain gray level patches.
- directional hysteresis due to the raster order of processing (most apparent in very light and very dark areas), and
- transient behavior near edges or boundaries.

2.2.1 Correlated artifacts

Halftoned images of uniform gray levels processed by standard error diffusion are shown in Figure (2.1). The level $\frac{I_0}{8}$ is shown at the top left and increasing levels with a step of $\frac{I_0}{8}$ are alternately placed at the right and the left side. The correlated non-uniform artifacts

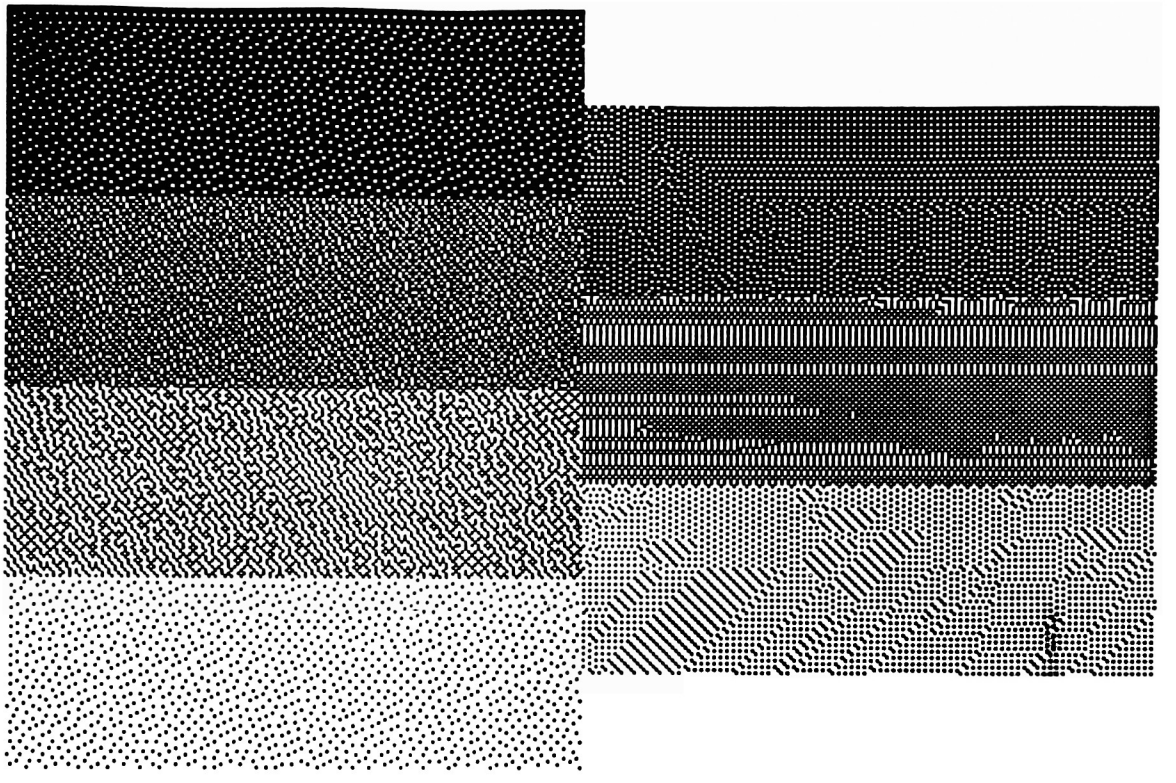

Figure 2.1: Constant gray levels (multiples of 1/8) processed by error diffusion.

disturb the perception of a smooth output and have different character for different image intensities. In this sense error diffusion discriminates in gray level. An example of a 'good' representation is the level $I_{max} * \frac{7}{8}$ while $\frac{I_{max}}{4}$ is poorly represented by this halftone process. The uniformity of the reproduction by a binary process has been quantified by [Uli87] by a measurement of anisotropy: *i.e.* the relative variance of frequency samples within two concentric circles which have radii f_r and $f_{r+\delta r}$:

$$A(x) = \frac{s^2(f_r)}{P_r^2(f_r)}, \tag{2.4}$$

where $P_r^2(f_r)$, is a radially averaged power at representative f_r, and $s^2(f_r)$ is the unbiased sample variance for the same radial frequency band. The anisotropy curves are shown for the gray levels of Figure (2.2). A measure greater than 0 dB indicates a specially anisotropic pattern; this level is clearly exceeded for $I = \frac{I_{max}}{4}$.

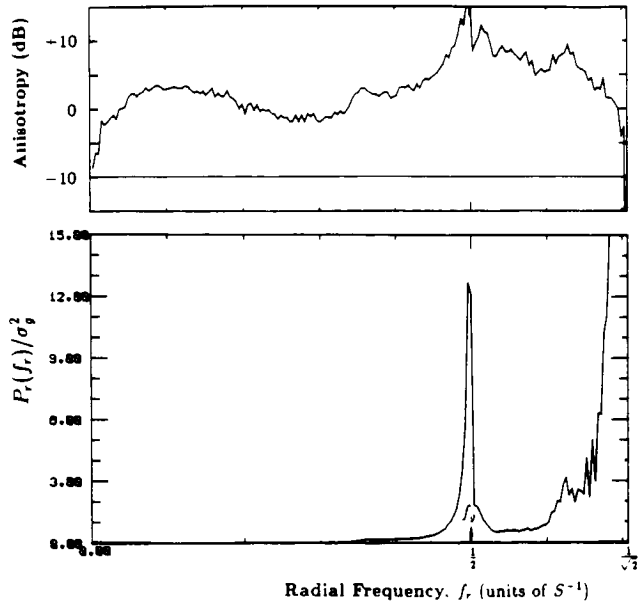

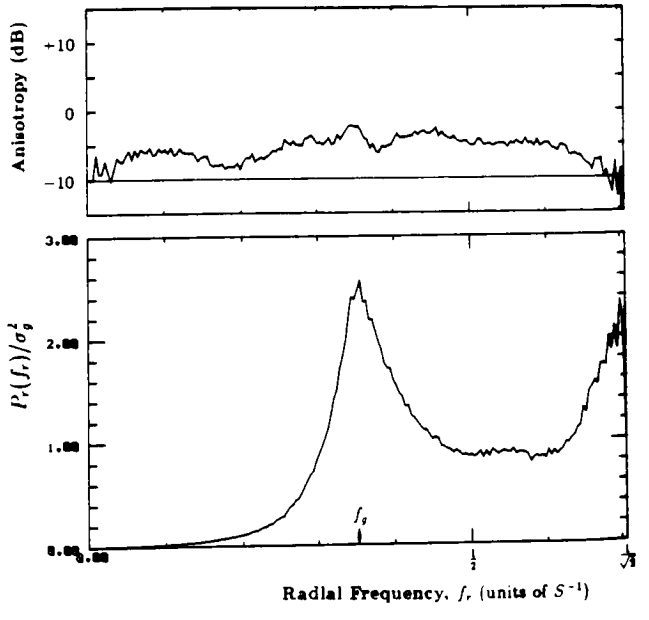

Figure 2.2: Anisotropy curves for graylevel (1/4) I(max) and 7/8 I(max) at bottom (Figure taken from [Uli87])

2.2.2 Directional hysteresis

The correlated artifacts appear as aligned "worms" with some preference for diagonal directions. Although this effect is very similar to the correlated artifact, it is not linked to specific gray levels but is due to the directional order of processing and the choice of weights. A suggestion of how to avoid this type of correlation is to use a different order of processing, *e.g.* along a space filling curve, such as the Peano curve [WN82]. The texture artifact can also be reduced by randomly switching the weights during processing [KMNK89].

2.2.3 Transient behavior

The transient behavior near edges (left and top) of the image can be eliminated by changing the starting conditions at each scanline. Instead of resetting the error to zero at the start of each scanline, the image is treated as a long one-dimensional array so that the error created at the last pixel of one row will be passed to the first pixel of the next row with a weight factor 'a'. In this way, a certain non-correlated error attenuates the transient artifacts at the left side of the image. Transients in the first scanline can be reduced by running error diffusion several times on it and inserting the errors created at the same position in the next run. Examples of the phenomenon of transient behavior and the two alternatives are given in Figure (2.3, 2.4).

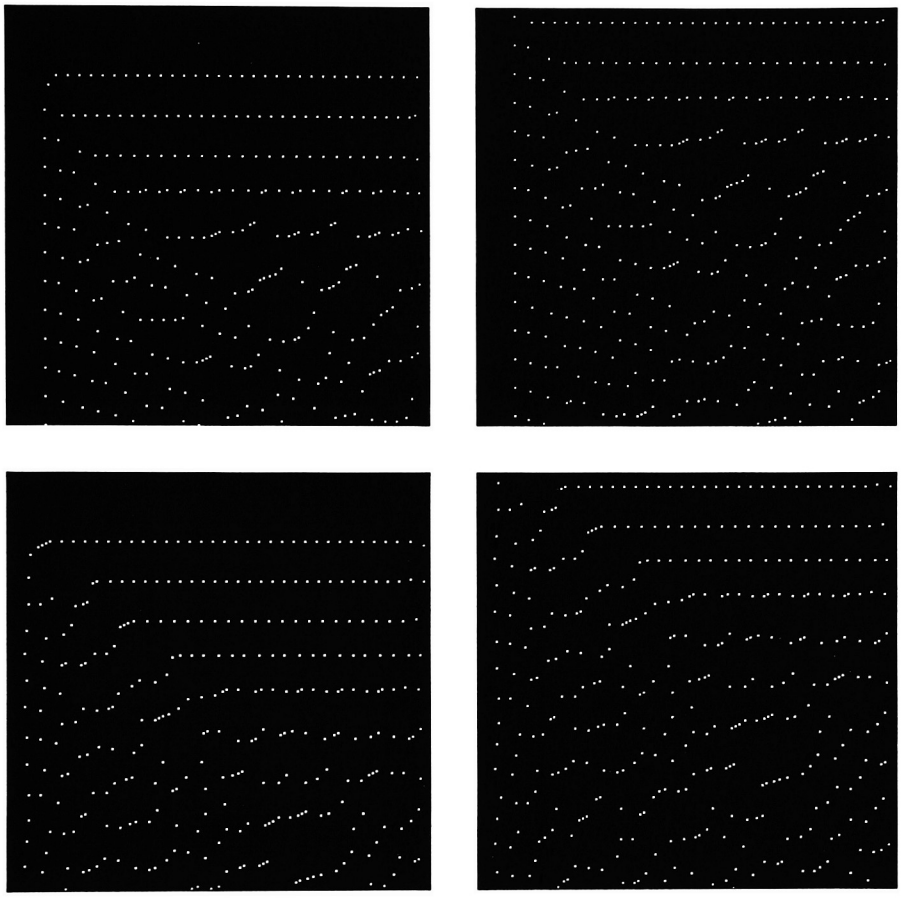

Figure 2.3: A constant level(= 2) processed by ED (top left), ED with wrap around error (bottom left), ED with multiple processing of the first scanline (top right), ED with both adaptations (bottom right).

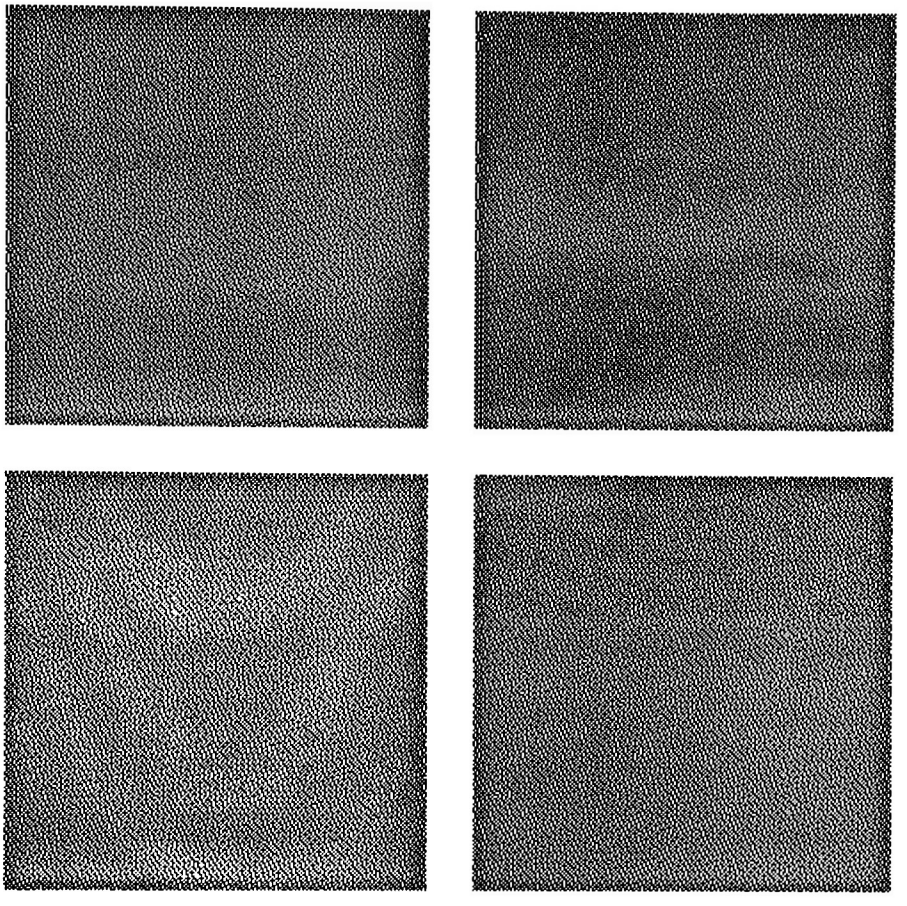

Figure 2.4: A constant level(= 100) processed by ED (top left), ED with wrap around error (bottom left), ED with multiple processing of the first scanline (top right), ED with both adaptations (bottom right)

2.3 Parameters

2.3.1 Weights

The weights obtained by Floyd and Steinberg were developed by trial and error to obtain the checkerboard for $I = \frac{I_{max}}{2}$; By changing the weights, one can change the direction of

the second artifact but that cannot remove it. Figure (2.5) indicates that the weights not only affect the wormlike structure, but influence the transient behavior as well. One could propagate error over larger regions to reduce direct correlation artifacts. A 12-element neighborhood for error diffusion defined by Jarvis *et al.* [JJN76] is shown in Figure 2.6. The weights are normalized before use. The authors describe the improvement of the larger environment as a change in microstructure. Direct correlation is diminished, while the general characteristics of error diffusion are maintained. Ulichney remarks that the directional hysteresis has increased for the very dark and light areas, while pixels are clustered more in the middle gray region (between 0.33 and 0.66) [FS86]

The function of the weights has been studied closely in one dimension by Manfred Broja *et al.* [BEB86]. A two-weight diffusion which distributes the errors to the adjacent neighbor (a) and the neighbor two pixels distant (b) reproduces the correct gray level for $a + b = 1$. Even in this case, instabilities can appear because the absolute value of the cumulative error can become so large that the algorithm collapses. If the error increases monotonically, the process will produce only uniformly black or white outputs or will alternate between black and white until the maximum of the computer dynamic range is reached. The region in the a-b-plane that satisfies $|a| + |b| \leq 1$ is free of instabilities. The output image which is processed by 1-D ED with weights within the region $|a| + |b| < 1$ gives the impression of a quantized image (Figures 2.7,2.8) where each quantization level is built up of a more or less fixed pattern of black and white pixels. The number of possible quantization levels was not predicted, but seems to be related to the choice of the weights.

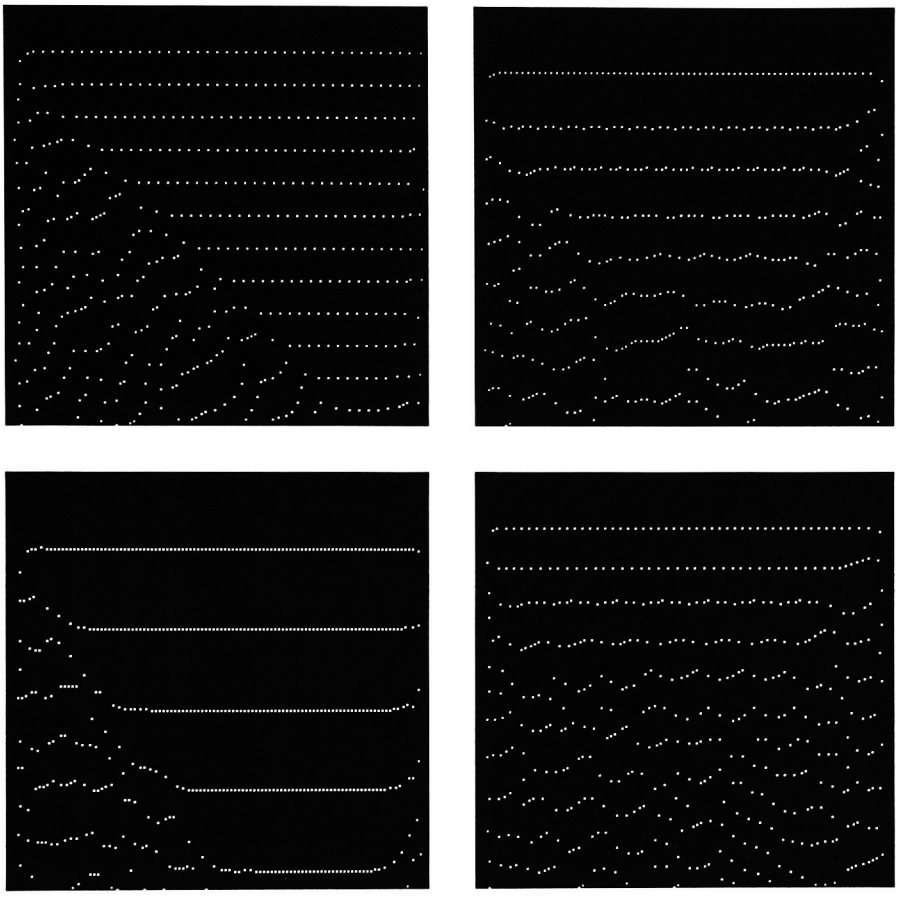

Figure 2.5: A constant level(= 2) processed by ED with set of weights 7 1 5 3 (top left), 1 7 3 5(bottom left), 3 5 1 7 (top right), 5 3 1 7(bottom right)

		.	7	5
3	5	7	5	3
1	3	5	3	1

Figure 2.6: 12-element neighborhood, for ED by Jarvis *et al.*

2.3.2 Threshold

Instead of experimenting with the weights, variations on ED may change the threshold to break up the correlated patterns. A small variation in threshold has been suggested by Fawcett and Schrack [FS86] to break up the very specific patterns when the weights defined by Jarvis [JJN76] are used. The threshold is changed to 0.33 and 0.66 if the result previous to the currently processed pixel was a five-pixel sequence with respective binary output: | 1 | 0 | 0 | 1 | 0 | or | 0 | 1 | 1 | 0 | 1 |. The threshold for all other cases remains at 0.5. This variation is called pattern inhibition.

A periodic threshold adaptation has been proposed [BHB83] which adds a dither mask weighted by a certain factor α to the original threshold level $\frac{I_{max}}{2}$ so that the final threshold range lies in the interval $[T - \frac{\alpha}{2}, T + \frac{\alpha}{2}]$. For this purpose the ring-shaped screen[Bry78] seems to be appropriate. Although the wormlike structures are disrupted, the image loses some of its sharpness.

An image-dependent threshold introduced in 2-D error diffusion [EK91] will enhance edges in the output. The amount of information compared to the threshold will be controlled by a weight factor K, and therefore the decision threshold for clipping is adapted to:

$$B_{ED} = step(\tilde{I}(x,y) - T) \tag{2.5}$$

and with the error diffusion weights indicated by α_{ij} the modified input transforms into

$$\tilde{I}(x,y) = KI(x,y) + \sum_{ij} \alpha_{ij} E(x+i, y+j), \tag{2.6}$$

while the error is still calculated in the same way as in standard ED:

$$E(x,y) = [I(x,y) + \sum_{ij} \alpha_{ij} E(x+i, y+j)] - B(x,y) \tag{2.7}$$

in order to obtain the same integrated gray level in output and input. The Figures (2.9,2.10,2.11) demonstrate the impact of the parameter K on the sharpness of the image.

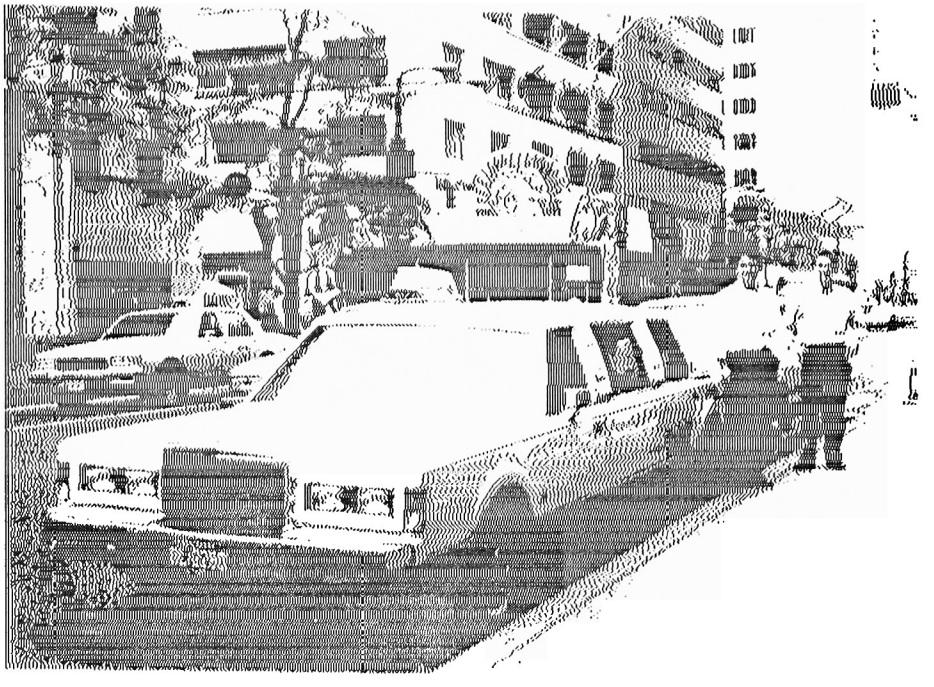

Figure 2.7: 1D-ED with weights a = 0.8 and b=-0.2

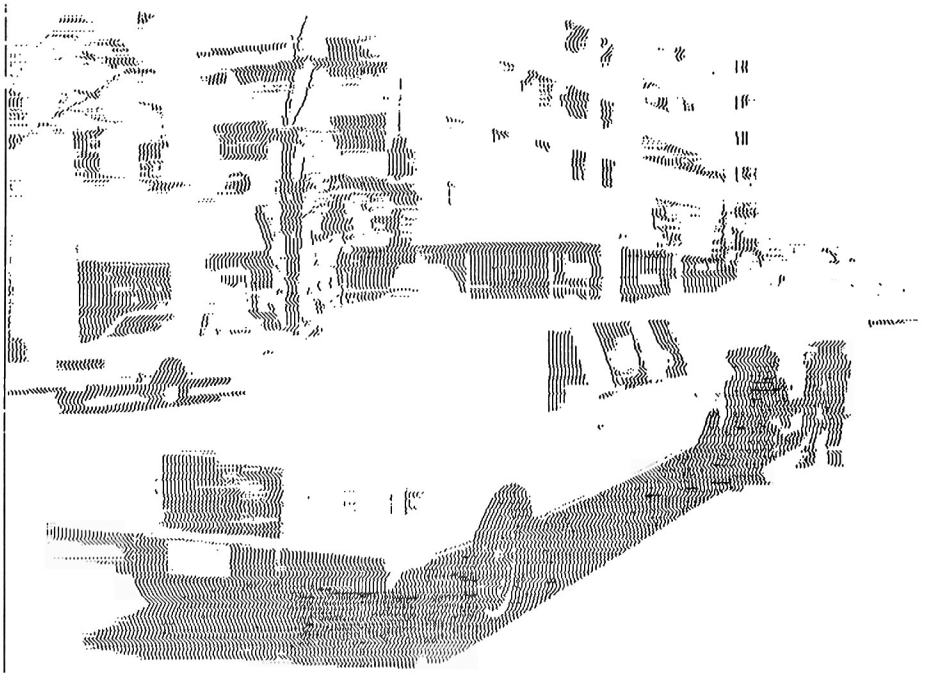

Figure 2.8: 1D-ED with weights a = 0.7 and b=-0.3

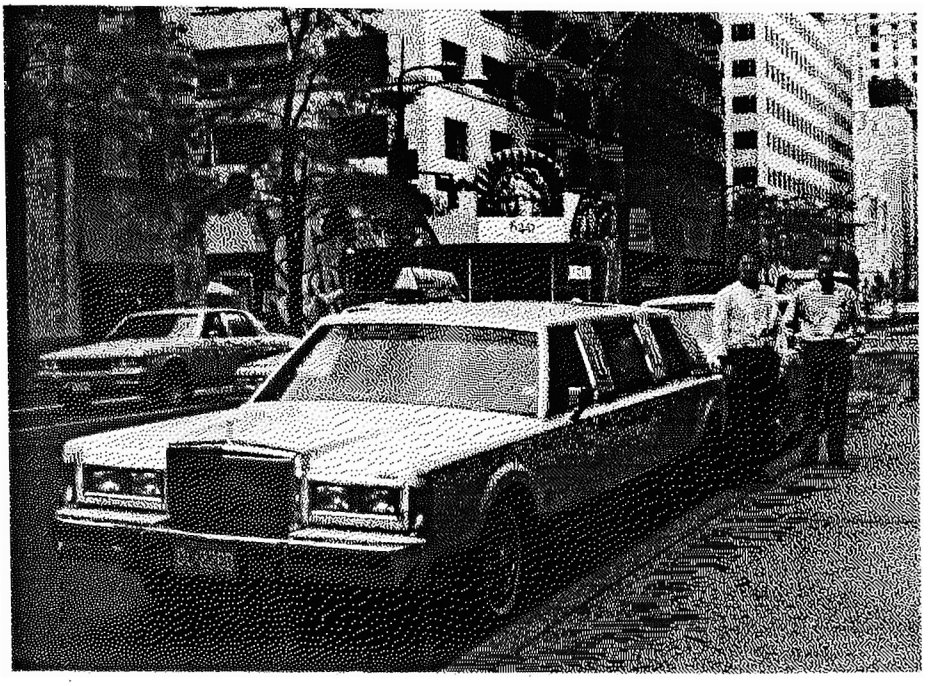

Figure 2.9: Error diffusion with threshold parameter K = 1.

Figure 2.10: Error diffusion with threshold parameter K = 0.1

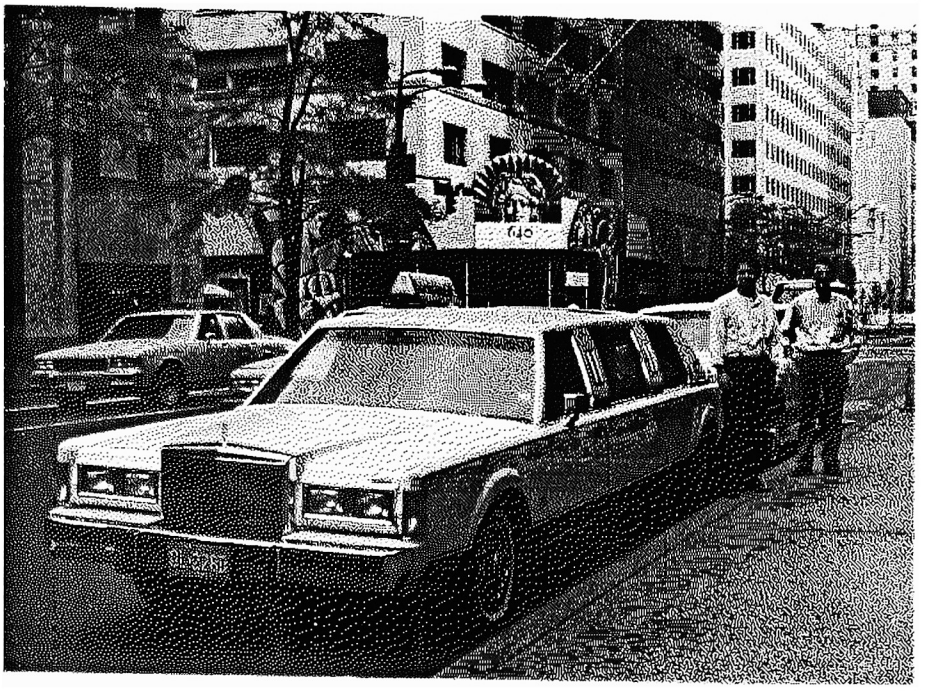

Figure 2.11: Error diffusion with threshold parameter K = 2.

$K = 1$ is standard error diffusion, while $K > 1$ leads to edge enhancement with increasing strength for larger K. For $K < 1$, the image appears less sharp, as less information is inserted in the system. The description above is equivalent to the standard error diffusion if an image-dependent threshold is substituted for the fixed threshold T:

$$T(x, y) = T + (1 - K)I(x, y). \tag{2.8}$$

This is derived by substituting (2.6) in (2.5) and comparing to the result of standard error diffusion (2.3). This type of edge enhancement appears to have little sensitivity to noise when compared to other imaging techniques. This is because the sum of the gray levels is always preserved, while different choices of K affect only the micro-structure. A more detailed analysis of the effect of the threshold variation on transitions between gray levels is shown in Fig.(2.12). Each image consists of 4 patches of level $\frac{1}{8}$ and $\frac{5}{8}$ on the first row, and $\frac{7}{8}$ and $\frac{3}{8}$ on the second row. This test pattern allows us to evaluate the edge response at both horizontal and vertical edges for upward and downward transitions of the same

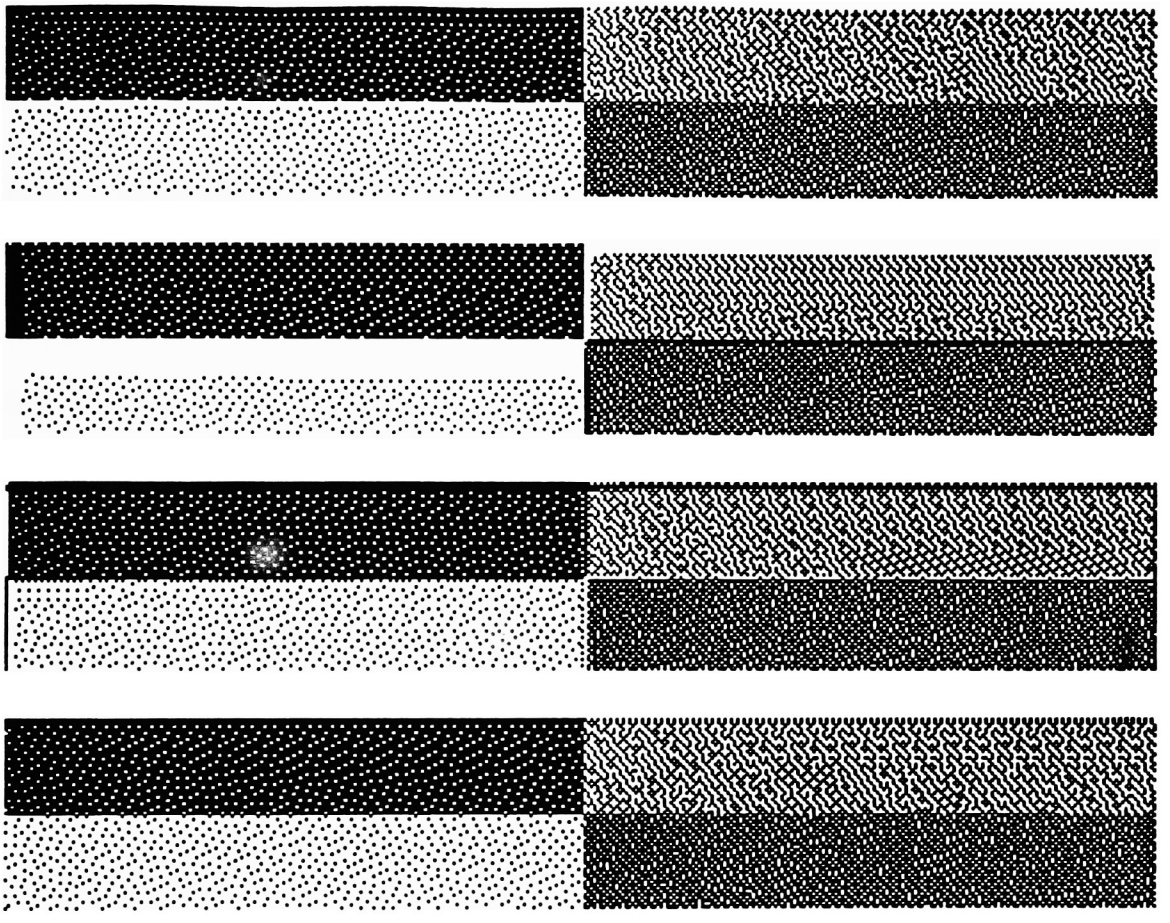

Figure 2.12: Test pattern processed by varying threshold, with parameters K= 1.0, 4.0, -2.0 and 0.5

magnitude. The first image shows the result of standard error diffusion; the other three images are processed by error diffusion with threshold variation with $K = 4.0, -2.0$, and 0.5. The large positive value of K, results in strong edge enhancement as evidenced by the white bar visible at both horizontal and vertical transitions toward a lower intensity level and a black bar for the opposite transition. The negative value $K = -2.0$ produces similar bars with reversal contrast but not as visible. A shadow bar of opposite binary output appears next to these. For $K = 0.5$, a slight blurring effect can be seen, when compared to

the original ED version with K = 1.

2.3.3 Impulse response

A very attractive aspect of error diffusion is that it displays intrinsic edge enhancement which has been described as lateral inhibition. This is one of the main reasons for its good reproduction of fine detail. This type of edge enhancement has been statistically evaluated by K.Knox [Kno89], who calculated the parameters of an equivalent unsharp mask. The analysis averaged vertically aligned gray steps processed by error diffusion over several scan lines, and was repeated for a large number of steps of different amplitude. The sharpening of vertical edges can be observed in the top image of Figure 2.12. The equivalent one-dimensional mask of the vertical edge enhancement in 2-D ED exhibits asymmetry, as shown in Figure 2.13. The average output of ED, $y(x)$, is predicted to be:

$$y(x) = \frac{I(x) - K(I(x) * b(x))}{1 - K} \tag{2.9}$$

with b(x) shown in 2.13.

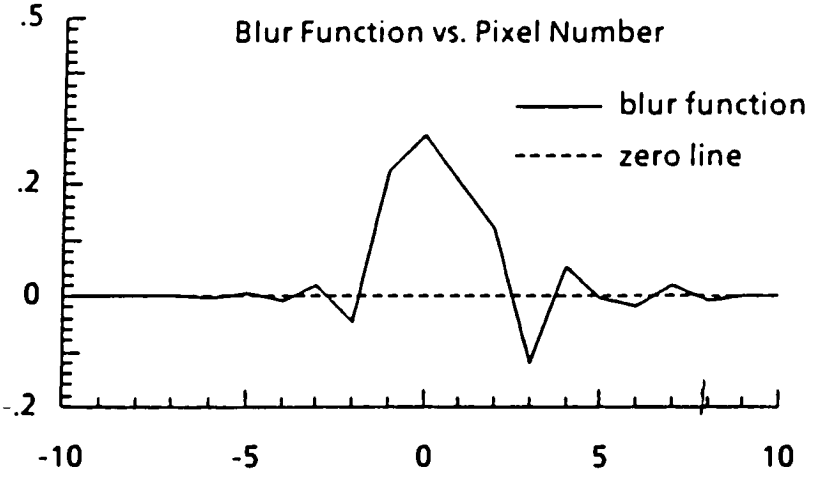

Figure 2.13: Equivalent blur function for the unsharp masking of vertical edges in ED (Figure taken from [Kno89])

2.4 Approaches to modeling ED

As already described, the values of the weights and modulation of the threshold might have important influence on the performance of error diffusion. From this review, it is clear that the majority of the modifications to ED have been made on a heuristic basis, rather than on a firm mathematical basis. The modelling of error diffusion is particularly difficult because of the non-linearity of thresholding and thus attempts to understand it have been approached by quite different methods.

2.4.1 Statistical approach

One statistical study of ED was performed by Barnard [Bar88]. A statistical expression was derived for the estimate of error between input and output as a function of the weights. The dependence of the variance of the Fourier transform of the error function on the weights of ED is described. The process can be optimized by solving the linear equations which express the derivatives of the variance on these weighting parameters. This probabilistic model assumes that the errors E(n) and E(n-1) are uncorrelated and that E(n) is independent of the input intensity. When the first assumption is violated, a much more complex expression needs to be evaluated. In Figure (2.14), the negative errors are shown by adding 127.5 and applying regular dithering. The strong correlation with the original image shows that the second assumption is clearly violated. A correlation between E(n) and I(n) also strongly implies that E(n) and E(n - 1) are correlated similar to I(n) and I(n - 1). The general case with four weights was not treated. Still, it was shown that large weights distributed in one direction generate errors (between input and output) with high power in the frequency domain in a band along the perpendicular direction. The error was shown to increase at higher frequencies, and is therefore sometimes called blue noise[Uli87].

2.4.2 Linear filter approach

Several theories have been developed to describe the performance of error diffusion or the noise it creates as a first order approximation of an equivalent linear system. This simple approach is sufficient to describe the behavior of the noise in frequency domain and is therefore used to reduce binarization noise in the reconstruction plane of a CGH [vdB90, WWB90]. The error in the Fourier domain could be localized as a function of the weights. In this approach, no assumptions are made about correlations between the input I(n) and the error E(n), nor about the relation between E(n) and E(n-1). In this sense, the approach is more rigorous than the statistical model described before.

Sullivan and Miller [SM90] include a filter that represents the lowpass character of the eye in the decision of the binary output in standard error diffusion. The modified input is compared to the two possible output values, as perceived in the environment of 24 previously obtained outputs, and filtered by the lowpass eye. The perceived binary value which best approximates the modified input is accepted. The errors are calculated in the same way. A flow chart diagram of the procedure is given in Figure (2.16), while the filter values for a 400 dpi resolution device are listed in Figure (2.15). This filter reduces the modified error diffusion algorithm to the original if all filter weights but the center are zero. The anisotropy of the filter reflects the lower sensitivity of the eye in diagonal directions, and the lowpass character of the filter will reduce highly visible lowpass errors while permitting blue noise to pass.

2.4.3 Analytical approach

The analytical description for error diffusion has been given in one dimension [EH84] as a pulse density modulation generated from a frequency modulation.The ED is considered to be a sampled version of this output function. The binary output is the result of clipping the

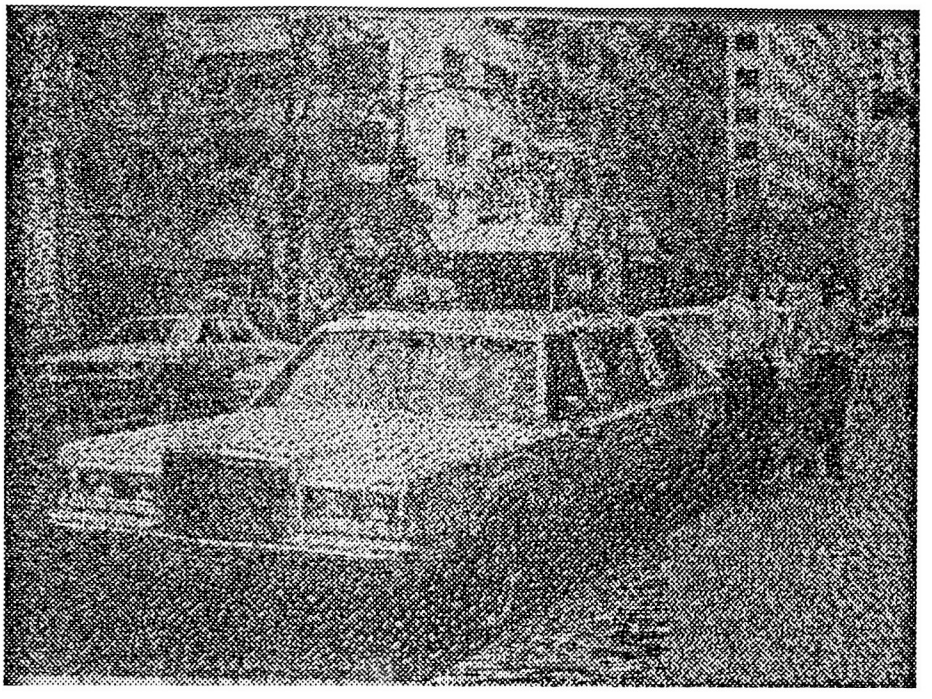

Figure 2.14: The negative error as occurring in ED

-0.009	-0.010	0.004	0.021	0.004	-0.010	-0.009
-0.010	-0.019	0.007	0.051	0.007	-0.019	-0.010
0.004	0.007	0.079	0.190	0.079	0.007	0.004
0.021	0.051	0.190	0.368			

Figure 2.15: Filter values used by Sullivan and Miller [SM90]

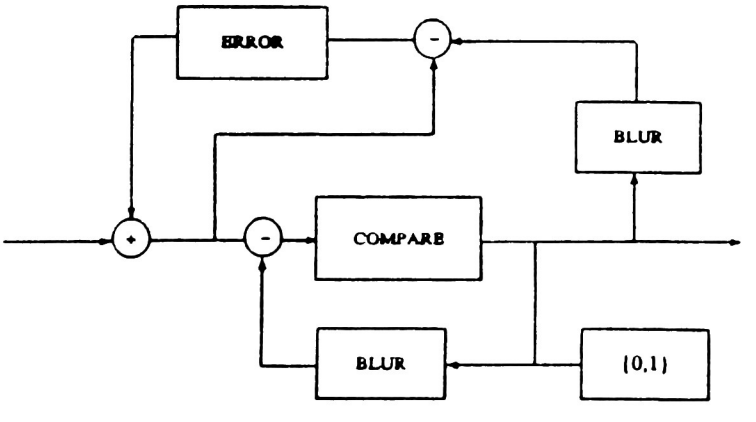

Figure 2.16: Extended ED scheme by Sullivan and Miller, taken from their article [SM90]

carrier $C(x)$ by a threshold $T(x)$, where:

$$C(x) = cos[\frac{2\pi}{\lambda I_0}(\int_0^x I(u)du + \phi_0)] \tag{2.10}$$

and

$$T(x) = cos[\pi \frac{I(x)}{I_0}]. \tag{2.11}$$

The result is:

$$B(x) = step[C(x) - T(x)]. \tag{2.12}$$

The derivative of the argument of the carrier wave cosine will determine the density of the pulses. The dependence of the threshold on the input (2.11) assures that the width of the pulse is fixed. Other binarization methods can be extracted by similar descriptions: fixed pulse frequency and variable pulse width, variable pulse frequency and fixed pulse width(PDM), variable pulse frequency and width [EH85].

PDM has been extended to two dimensions by generalizing the integral in the carrier. In the 1D case, the carrier (2.10) contains the one-dimensional integral of the input which will determine the density of the pixels in the direction of the scan. The constraints for two dimensions require that the carrier determines both horizontal and vertical density. In [EH87b], the 1-D integral is replaced by a 2-D integral

$$\int\int_{A_m} I(x,y)dxdy. \tag{2.13}$$

The shape of the integrated area A_m defines the configuration of the pulses, and it is thus impossible to maintain the simple order of processing, *i.e.* scanline by scanline. In this sense, the two-dimensional PDM is not a model for error diffusion but a binarization method in its own right.

A refinement of 2-D PDM is obtained by positioning pulses in the area with mean gray level equal to one pulse, and locating the pulse according to a specified moment of the

input gray level. The momentis of order P of the input intensity in Area A_m, in the x and y direction are:

$$x_{c,m}^{P} = \frac{\int\int_{A_m} xI^{P}(x,y)dxdy}{Q_m} \tag{2.14}$$

and

$$y_{c,m}^{P} = \frac{\int\int_{A_m} yI^{P}(x,y)dxdy}{Q_m} \tag{2.15}$$

where

$$Q_m = \int\int_{A_m} I^{P}(x,y)dxdy \tag{2.16}$$

This additional freedom results in some level of control of the contrast and edge enhancement.

A combination of PDM and error diffusion [Esc90] takes advantage of the fact that both algorithms perform best for different values of input intensities. Error diffusion is used for $\frac{1}{4} \leq I \leq \frac{3}{4}$, while intensities at the extrema $I < \frac{1}{4}$ or $I > \frac{3}{4}$ are processed by PDM. The image produced by this process differs from ED only in the very light or dark areas (see Figures 2.17, 2.18)

2.4.4 Thesis approach

The previous paragraph, which contained the only analytical approach to describe one-dimensional version of error diffusion, will be the point of departure for an investigation of threshold modulation. The threshold variation was shown to have a positive influence on the performance of the algorithm in that it is able to sharpen the overall image. Because edge enhancement has a significant effect on perceived image quality, it must be well understood and controllable. Although one-dimensional ED does not include several parameters that are present in its two-dimensional equivalent, the investigation of the 1-D case might contribute to understanding of the more complex 2-D case. This attitude however has been cast doubt on before[Bar88].

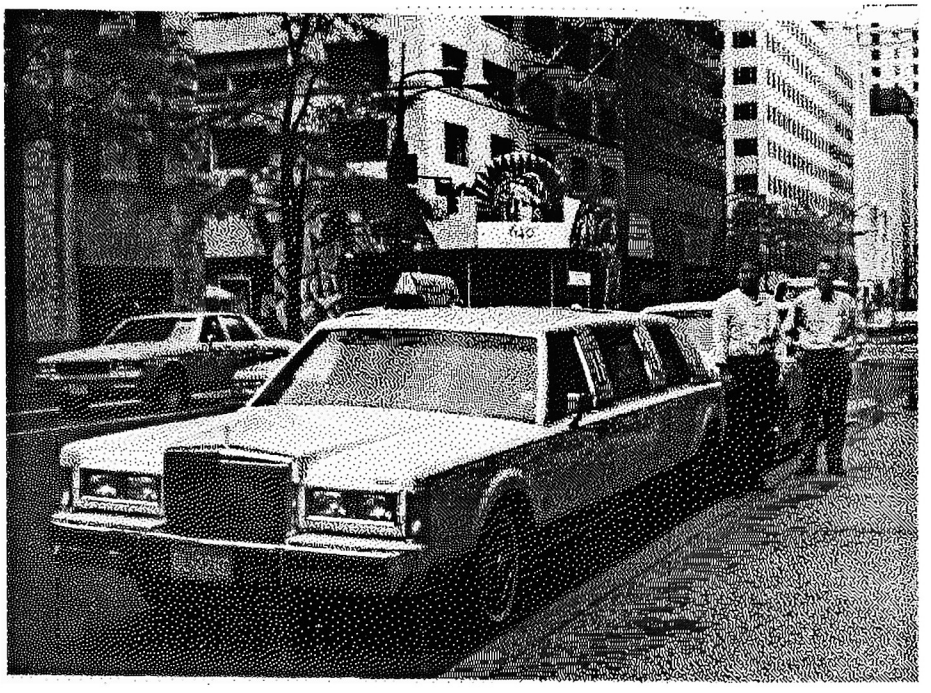

Figure 2.17: Combination of PDM and ED

Figure 2.18: Standard ED

Chapter 3

PDM as a Model for ED

As already described, 1-D ED is a numerical method that transfers a quantized input defined on a fixed grid to a binary output. In contrast, pulse density modulation is an analytical description for a binarization process of a continuous input. The result of both methods have been shown to be similar when the output of PDM is sampled on the same grid as ED [EH84].

3.1 Construction of PDM

The idea of using a frequency modulation to generate a pulse density modulation (PDM) as a model for ED, originates from the observation that the frequency at which pixels are turned on in ED is proportional to the input level for a constant input (Figures 2.1,3.1). In standard error diffusion, an input of level $\frac{1}{4}I_0$, will turn on one pixel out of four in a 2x2 area on the average (Figure 2.1); for 1-D ED, the same level is represented by one white output on a 4-pixel array in one row (Figure 3.1). Notice the wraparound error generated during processing.

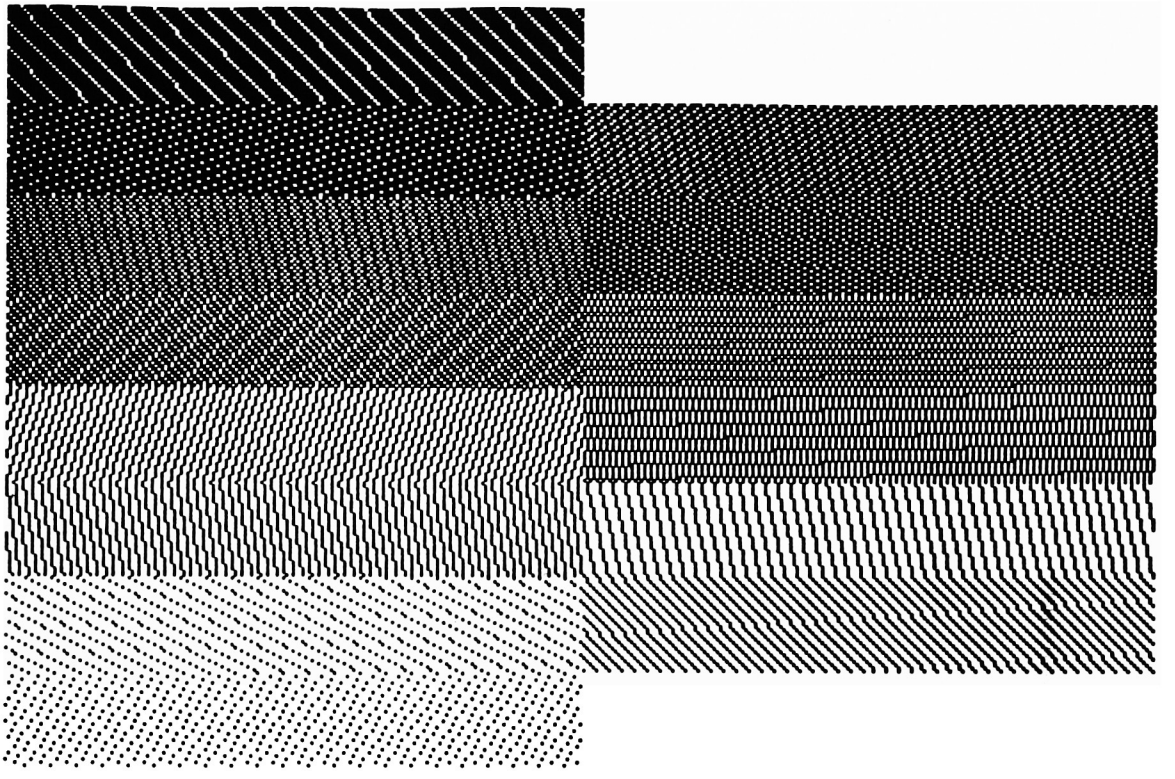

Figure 3.1: Constant gray levels (multiples of 1/8) processed by 1-D error diffusion.

A general binary pulse modulation applies a threshold $T(x)$ to a carrier $C(x)$:

$$B(x) = step\{C(x) - T(x)\}. \tag{3.1}$$

For PDM of a constant input, the carrier frequency is proportional to the input level I(x). To generalize PDM to a varying input, the local frequency is generated to be proportional to the input. The local frequency $\nu(x)$ is the derivative of the phase:

$$\nu(x) = \frac{\partial \phi}{\partial x} \sim I(x) \tag{3.2}$$

or

$$\phi(x) \sim \int_0^x I(u)du. \tag{3.3}$$

For the simplest form of a periodic carrier, a trigonometric function is chosen

$$C(x) = cos(k \int_0^x I(u)du) \tag{3.4}$$

The carrier

The constant k will be determined by defining the maximum frequency ν (or a minimal inherent wavelength λ) of the carrier for the maximum input I_0. The carrier should equal $cos(2\pi\nu x)$, while the general expression (3.4) reduces to $cos(kI_0x)$ for the same input. By solving the value for k and substituting in the general expression (3.4), the carrier is completely defined as

$$C(x) = cos\{\frac{2\pi}{\lambda I_0}(\int_0^x I(u)du)\} \tag{3.5}$$

The threshold

A second constraint will determine the threshold function, once the carrier has been defined. This additional requirement relies on the filtering property of the eye: the average input intensity should equal the average of the binary output over one period of the carrier function

$$\int B(x)dx = \frac{I_1}{\nu I_0} = \frac{\lambda I_1}{I_0} = \lambda\beta, \tag{3.6}$$

with I_1 assumed to be constant over the period considered, and $\beta = \frac{I_1}{I_0}$. In [EH85], the threshold is shown to be $cos(\frac{\pi I(x)}{I_0})$ for our choice of carrier in eq. (3.5).

Substituting the threshold and carrier information (3.5) into (3.1) gives the complete expression for the PDM:

$$B_{PDM}(x) = step\{cos[\frac{2\pi}{\lambda I_0}(\int_0^x I(u)du + \phi_0)] - cos[\frac{\pi I(x)}{I_0}]\} \tag{3.7}$$

which produces binary pulses of fixed width λ, at a frequency proportional to the input function. This statement is strictly true for a constant and a linear input. The construction of the pulse sequence by generating an input-dependent carrier and threshold is shown in Figures (3.2,3.3,3.4), for constant, linear and square wave input functions.

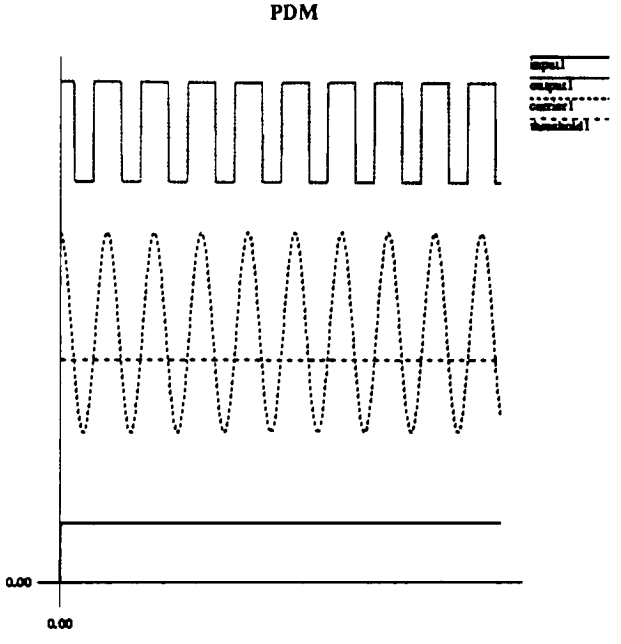

Figure 3.2: PDM created by cosine threshold

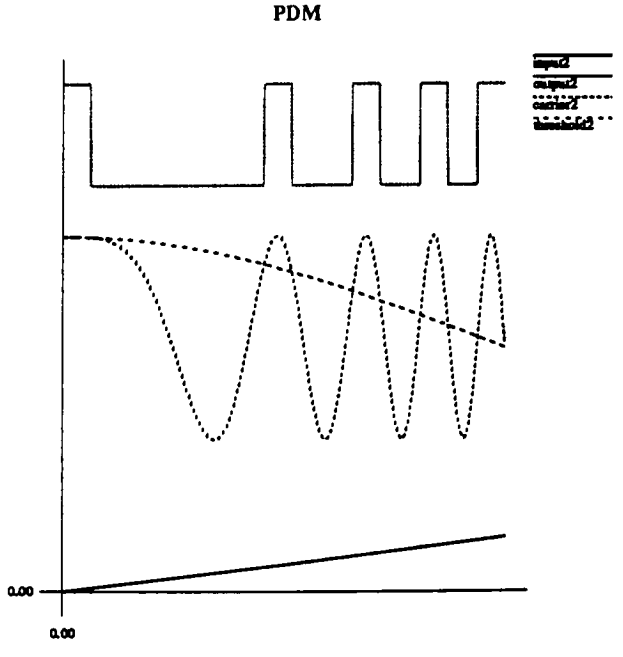

Figure 3.3: PDM created by cosine threshold

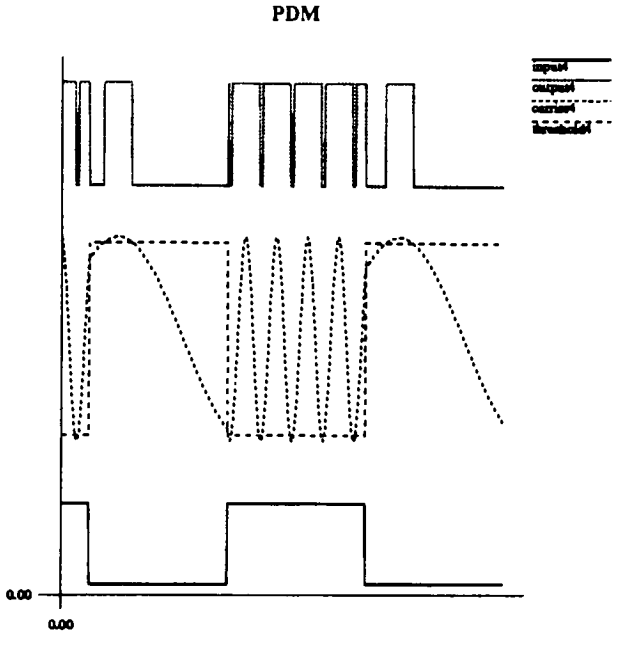

Figure 3.4: PDM created by cosine threshold

3.1.1 Constant input

If for example the input is a constant at the maximum level I_0, then the expression (3.7) reduces to:

$$B_{PDM}(x) = step[cos(\frac{2\pi x}{\lambda}) - cos(\pi)]. \tag{3.8}$$

Independent of the constant λ chosen, this is the shortest wavelength or the highest frequency obtainable for the carrier, and it will always exceed or equal the cosine threshold of $cos(\pi) = -1$. Therefore the binary output for the maximum input will be uniformly white, as required. The result for a general constant input I_1, is obtained by using the factor $\beta = \frac{I_1}{I_0}$, which represents the input level relative to the maximum. The expression (3.7)

becomes:

$$B_{PDM}(x) = step[cos(\frac{2\pi\beta x}{\lambda}) - cos(\pi\beta)]. \tag{3.9}$$

The carrier wavelength is $\frac{\lambda}{\beta} > \lambda$, which implies a frequency $\nu \sim \beta \sim I$. The fraction of the wavelength which will produce a white output, is determined by the threshold and for one cycle will correspond to the ratio of the threshold sector($-\pi\beta \leq$angle$\leq \pi\beta$) to a full cycle :$\frac{2\pi\beta}{2\pi} = \beta$. As a result, the white pulse which is the fraction ($= \beta$) of the wavelength ($= \frac{\lambda}{\beta}$) exceeding the threshold will have a constant width of size λ.

3.1.2 Alternative PDM

Some pulses may deviate in width from the expected wavelength λ, if there are discontinuities of the input as in Figure (3.4) . For a PDM described by (3.7) it is necessary for the input to vary slowly relative to the inherent wavelength of the frequency modulation.

In order to avoid disrupted pulses, a similar type of algorithm indicated as fixed block PDM (PDM_{fb}) can be constructed by attaching pulses of fixed width to the maxima of the carrier. The pulses can be described as the convolution of the fixed-width pulse (a rect) with a comb function centered on the carrier maxima x_i: rect function of fixed width:

$$B_{PDM_{fb}}(x) = rect(\frac{x}{\lambda}) * \sum \delta(x - x_i) \tag{3.10}$$

where x_i is defined by

$$cos(\frac{2\pi}{\lambda I_0}\int_0^{x_i} I(u)du) = 1 \tag{3.11}$$

The construction of this PDM_{fb} is given in Figures (3.5,3.6, 3.7) for the same set of inputs.

Although there is a difference between PDM and PDM_{fb} it is a subwavelength event which might be of minor importance when ED is modeled as a sampled version of

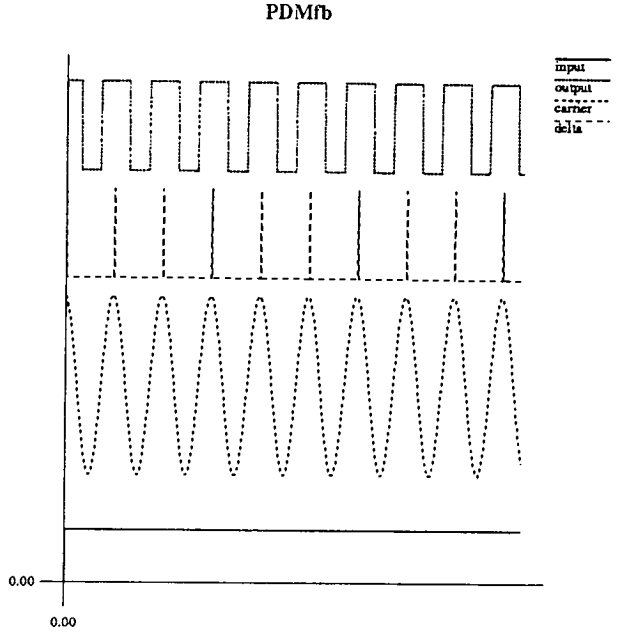

Figure 3.5: PDM by convolution for constant input

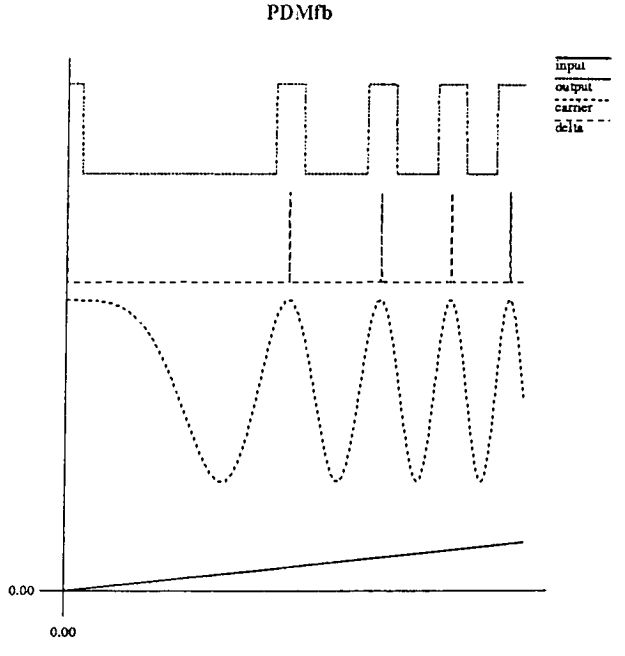

Figure 3.6: PDM by convolution for linear input

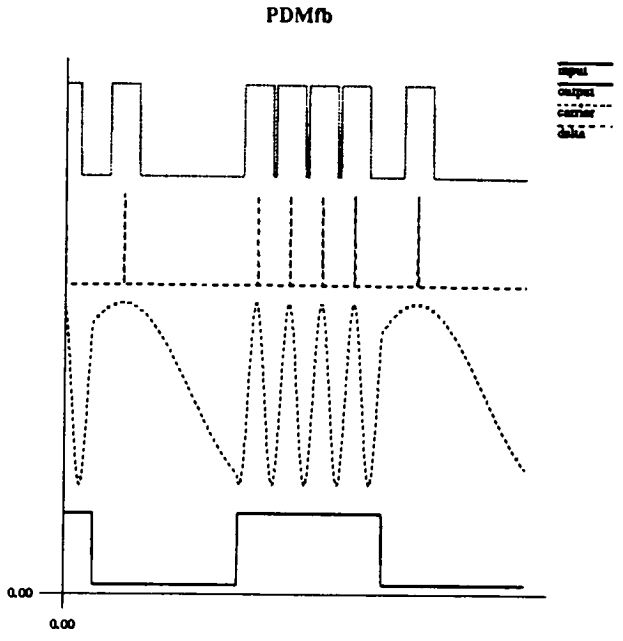

Figure 3.7: PDM by convolution for block pulse input

the frequency modulation and input varies slowly. From this point, only the analytical expression (eq. 3.7) will be considered as a realization of PDM.

3.2 1-D ED

The algorithm of Floyd and Steinberg can be applied to one dimension by transferring the error in one direction only, which is essentially the method designed by Hale [Hal76]. 1D-ED is a sequential process which transports a history-dependent error $E(n-1)$ from pixel $n-1$ to pixel n where it is added to the input, to create a modified input $\tilde{I}$:

$$\tilde{I}(n) = I(n) + E(n-1). \tag{3.12}$$

The binary output

$$B(n) = step(\tilde{I}(n) - T) \tag{3.13}$$

is set to '1' whenever the threshold T is exceeded. The difference between the modified input $\tilde{I}(n)$ and the binary output $B(n)$ is the error

$$E(n) = \tilde{I}(n) - step(\tilde{I}(n) - T), \tag{3.14}$$

to be carried over to pixel $n + 1$.

3.3 Comparison of ED and PDM

3.3.1 Integral versus error

The modified input (3.12) of 1-D ED is analogous to the integral in PDM, in that both contain history-dependent information. The modified input in ED contains the error transferred from the previous pixel, and was again dependent on previous inputs.

3.3.2 Threshold versus phase

According to [EH84], the threshold T in ED corresponds to a starting phase $(-\phi_0)$ in PDM. A different threshold in ED generates an image with a different microstructure but the same overall appearance. An example is illustrated in Figure (3.9) which represents an input image with increasing contrast towards the bottom and increasing frequency toward the right. The difference in structure due to different starting errors is mostly visible at low contrasts, and low frequencies. In PDM, the argument of the carrier defines a specific angle which is compared to the circle sector $[-\frac{\pi I(x)}{I_0}, \frac{\pi I(x)}{I_0}]$ defined by the threshold cosine (3.7). If the angle belongs to that sector, the carrier cosine is bigger than the threshold cosine and the output results in a '1'. The argument of the carrier describes a continuous repositioning

Figure 3.8: 1D error diffusion

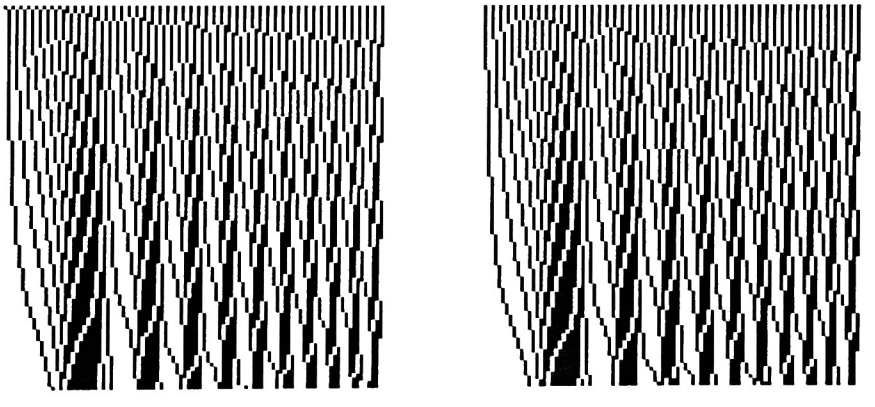

Figure 3.9: 2 different starting errors for ED

of the angle versus the threshold sector. Obviously, the additional phase will determine the starting point of the sequence of white pulses, and will affect the output, as the decision for the binary output refers to the relative positioning between threshold sector and integral. In the same sense we could express a more general PDM by using imaginary expressions for the carrier, while the threshold sector can be centered at any arbitrary angle ϕ_c:

$$C(x) = e^{i\phi(x)} \tag{3.15}$$

with

$$\phi(x) = \frac{2\pi}{\lambda I_0}(\int_0^x I(u)du + \phi_0) \tag{3.16}$$

and

$$B_{PDM'} = 1 \Longleftrightarrow \phi(x) \in [\phi_c - \frac{\pi I(x)}{I_0}, \phi_c + \frac{\pi I(x)}{I_0}] \tag{3.17}$$

Because of the differential operation between the carrier angle and the threshold angle, it is obvious that starting error and threshold sector rotation have the same function.

We observe similar behavior for starting error and threshold, which are two parameters corresponding to the phase in PDM. ED will produce the first pulse as soon as

$$T \leq \sum_{k=0}^{n} I(k) + E(-1), \tag{3.18}$$

where $E(-1)$ is an arbitrary starting error, usually set to be zero. It is clear that a starting error $E(-1)$ in ED can have the same function as the threshold, but is now added to the other side of the inequality (3.18) and will act as if it has opposite sign. In this sense the threshold in ED corresponds to the positioning of threshold sector ϕ_c in the general PDM, and the starting error in ED takes the function of an additional phase in the carrier. As already mentioned, the action of ϕ_c and phase in PDM and of the threshold and starting error in ED are interchangeable if the sign is respected.

3.3.3 Incubation time

In ED, if $|T - E(-1)|$ exceeds the maximum value I_0, it may take several pixels with binary output "0" before the error is reduced to the normal range of $\pm 0.5 I_0$. From this point, ED is again able to switch between output states. This is referred to as "saturation" in general, or "incubation" if it occurs at the beginning of a line. Obviously, these will result in a loss of local information. Independent of the starting phase, PDM does not exhibit saturation because of its periodic character. Consider Figure (3.10) which shows images of uniform levels 100 and 200, processed with one dimensional error diffusion. The rows are processed independently, from left to right, and starting error increases with row number. As a result the saturation zone is depleted more for rows near the bottom of the image. To avoid artifacts caused by an out of range starting error, the starting error can be randomized so that the output probability of producing a 1 corresponds to the input gray level. Another more commonly used randomization transfers the error from the last pixel from previous row and uses this as a starting error. Similar techniques are used in 2D (see section 2).

3.4 Edge response

In [EH84] ED is related to PDM by the expression

$$B_{ED}(x) = B_{PDM}(x + \frac{d}{2}) comb(\frac{x}{d}) * rect(\frac{x}{d}) \tag{3.19}$$

where d is the space between sampling points and is analogous to λ, the minimum wavelength of the frequency modulation. Error diffusion is thus a sampled version of PDM, combined with a convolution with a rect function of width equal to the distance between pixels on the sampling grid. The phase shift of $\frac{d}{2}$ is needed due to the incubation time of ED, previously discussed. Comparison of ED and PDM can be simulated by

computer if the input function is assumed to be continuous (*i.e.* if it is sampled at a much higher rate for PDM). For example, a sampling rate of 50 times larger might be appropriate:

$$\text{sampling rate (PDM)} = 50 \times \text{sampling rate (ED)}.$$

In Figure(3.11), the construction of PDM is shown on a grid (input function = A; carrier = B; threshold = C). The thresholded carrier is shown in D, and is shifted over half the sampling interval d in E. The output of ED is shown in F, and is identical to E, which confirms (3.19).

The exact comparison of ED with PDM through (3.19) might fail if a continuous input is used for PDM, while ED requires a discrete set of input data.

In order to compare the performance of the two binarization methods, a one- dimensional average might give information for constant gray levels. For a constant level $\beta, (0 \leq \beta \leq 1)$, it will take a distance $\frac{\lambda}{\beta}$ to obtain one cycle for the carrier and to judge the right gray level. Therefore as the gray level of the original image changes from pixel to pixel, there is no fixed distance over which the gray level can be averaged in order to judge the response. One rather has to look for the probability of the binary output value that corresponds to the input level I(x) by studying the edge response.

The edge response of both methods has been studied by averaging the binary outputs over different starting conditions. The initial phase has been realized by varying ϕ_0 in the carrier (3.7) for PDM, while averaging over starting error $E(-1)$ in ED. To avoid an incubation time in ED, the range of initial modified input levels has to be adapted according to equation (3.18). PDM and 1-D ED both reproduce an input edge without any overshoots or undershoots when averaged over different starting phases and starting errors, respectively. However when the initial error is not adapted, there is an abrupt transition between saturation and the normal response to the input range. In case of an out-of-range input, the edge response of PDM results in aliasing. ED will similar to the starting error

problem, compensate for gray level error by saturating. As long as the overall graylevel cannot be compensated by producing I_0-levels (=binary output '1'), it will not be able to switch output. The reasoning is similar for $I_1 < 0$. Because the error in ED will be built up with maximum release of one I_1 unit, saturation is possible. In PDM, the difference between the modified input and output is always smaller than I_1, because of its cyclic behavior.

3.5 Conclusions

The outcome of the analytical analysis by comparing ED with PDM indicates that on average, 1D-ED represents the input perfectly (see paragraph about edge response) for values in the normal input range. This one-dimensional process does not correspond to its two-dimensional version which exhibits intrinsic edge enhancement. This provides an advantage in studying the edge enhancement created by threshold variation which is exclusively responsible for the non-ideal response. It was also shown that ED compensates immediately for out-of-range values by saturating as long as the overall integrated value of the output deviates from that of the input.

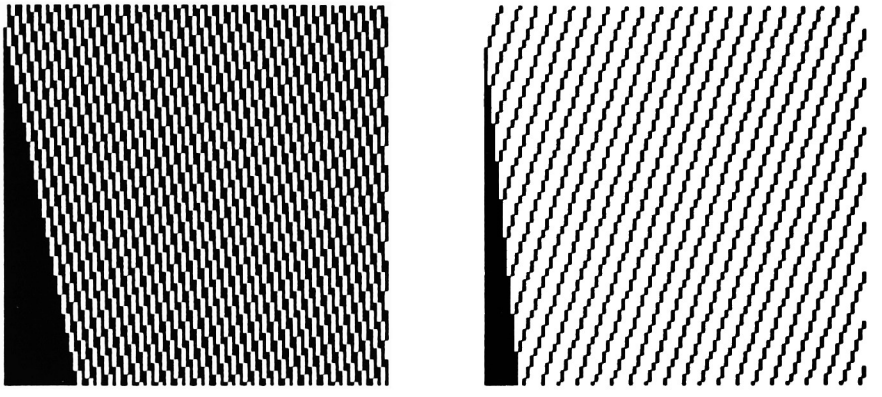

Figure 3.10: Varying starting error along the rows for ED causing different incubation time (input gray levels are 100 and 200)

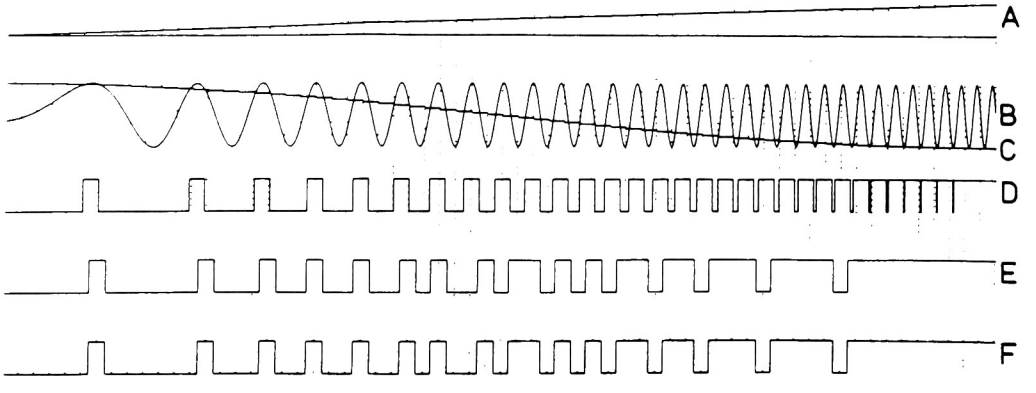

Figure 3.11: Construction of PDM(A, B, C), shifted(D), and compared to ED (Figure taken from [EH84])

Chapter 4

Threshold Modulation in 1-D ED

4.1 Edge enhancement in 1-D error diffusion by threshold variation

The images processed by 1-D error diffusion with threshold variation proportional to the input show similar edge enhancement to those processed by the enhanced Floyd algorithm. The examples (Figures 4.1, 4.2, 4.3, 4.4, 4.5, 4.6) present the results on scanned images for different values of the threshold constant c, where $T(x) = cI(x)$. The constant c is related to the previously defined K (equation 2.6) by $cI(n) = (1-K)I(n) + 127.5$. Since constant factors in the threshold cause only a phase shift and have no general effect on the output of an error-diffused image, the parameters c and $1-K$ are equivalent. For $c = 0.9(K = 0.1)$ blurring is hardly noticeable (negative edge enhancement), while in two dimensions this value of K clearly blurs the image content. For c = 0 we obtain the original image, and for $c = -1(K = 2)$, there is enhancement which is more pronounced for larger absolute value of c (*e.g.* $c = -50$). For positive values of c, the enhancement is reversed, which is especially clear for the large values $|c| = 50$. At edges between a brighter level at the left

Figure 4.1: Threshold = 0 I(x) gives the standard 1-D ED

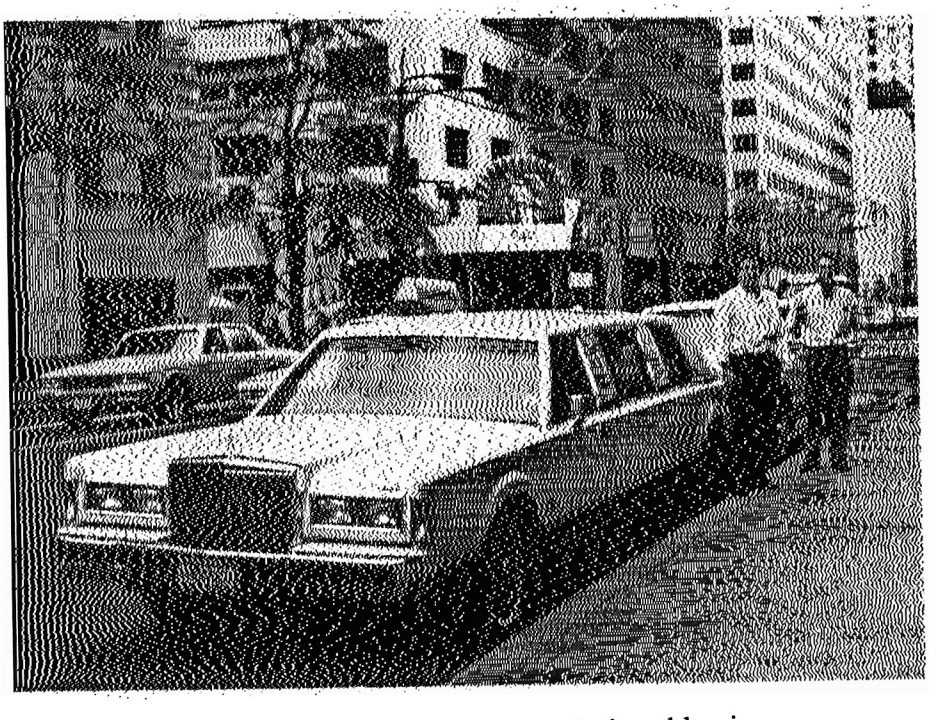

Figure 4.2: Threshold = 0.9 I(x) gives blurring

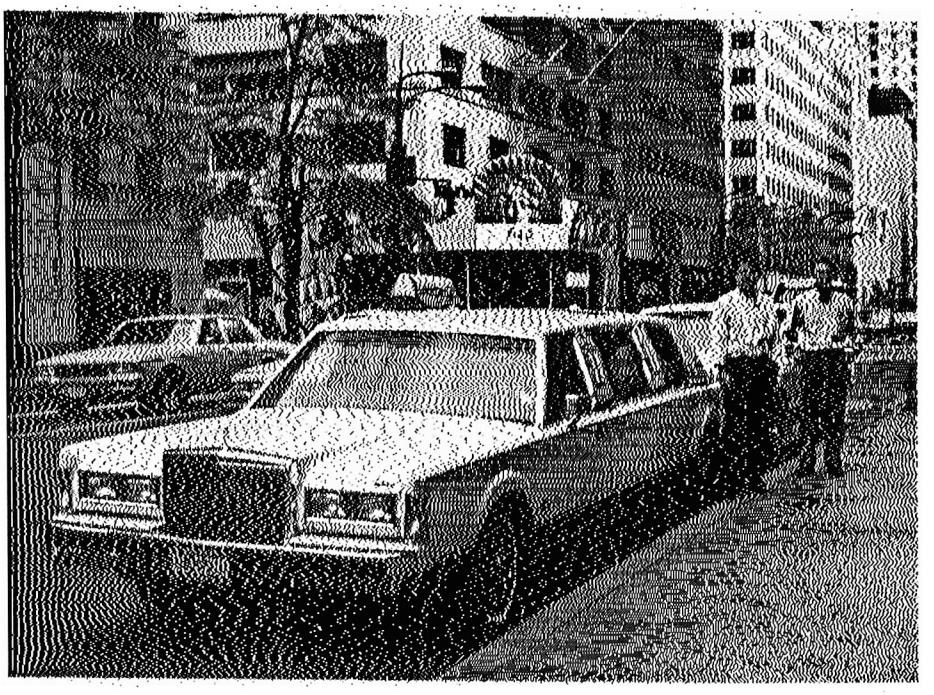

Figure 4.3: Threshold = -I(x)

Figure 4.4: Threshold = -50 I(x)

Figure 4.5: Threshold = +I(x)

Figure 4.6: Threshold = 50 I(x)

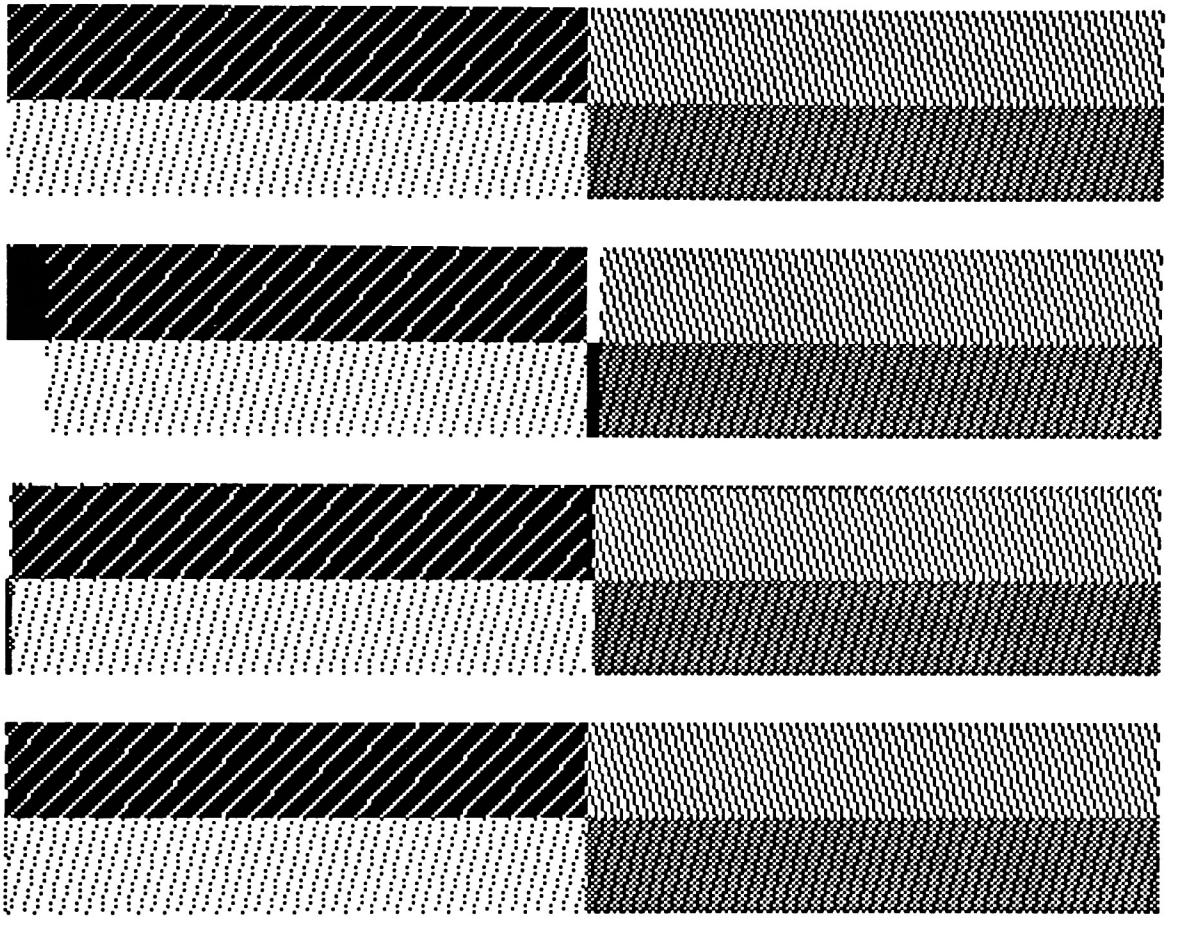

Figure 4.7: Test pattern processed by varying threshold, with parameters c = 0.0, -3.0, 3.0, 0.5.

and a darker level on the right, a white shadow is produced at the right side of the edge for a positive c (Figure 4.4), while it is a black shadow for the negative c (Figure 4.6).

Figure (Fig.4.7) shows the equivalent image as Figure (2.12) with transitions processed by 1-D error diffusion with threshold variation with c = 0.0, -3.0, 3.0, 0.5. Similar remarks are valid about the characters of the bars produced at the transitions, except of course that horizontal edges are not influenced because of the one-dimensional processing. The image was processed with wrap-around error transfer to avoid incubation at the left side. As a

consequence, we can also consider transitions of gray level between the end of a scanline, and the beginning of the next scanline. A negative c, gives the light shadow at a transition from dark to bright, and a black shadow for the opposite edge. A positive value of c produces narrower shadows of the opposite binary color. The additional bar observed in 2-D for small K's is not pronounced. The value c = 0.5 gives a different result from the c = 0 case, but only at a distance of one pixel from the edge, and is therefore not very noticeable or easily defined.

The edge response obtained by averaging the output of ED over starting error is also used as a third way to characterize the edge enhancement introduced by threshold variation. For a block input, the edge responses(Figures 4.8,4.9) show an asymmetric overshoot. For a negative value of c, the overshoot occurs at transitions to higher levels, while undershoot occurs only for negative changes of the input function. If the absolute value of c is increased, the height of the overshoot increases, until at a certain value of $|c|$, the maximum (minimum) is reached and the overshoot (undershoot) peaks start to broaden for still larger values of $|c|$. For negative values, the edge enhancement has the opposite direction of the overshoots mentioned above for positive values of c. The negative values are not completely complementary to the positive ones, because $|c|$ needs to be larger for $c < 0$ before enhancement occurs. For all values of $c \neq 0$ some new type of incubation time is observed, which increases for larger absolute values of the threshold parameter. To study this type of incubation time, the averaged output for a linear input was simulated as well for several values of the parameter (Figures 4.10,4.11, 4.12). In these figures both input and output had the same vertical offset. For negative c's the incubation time increases proportional to its absolute value. Apart from this event, the average output is shifted over a constant which seems to be related to the constant c which controls the edge enhancement.

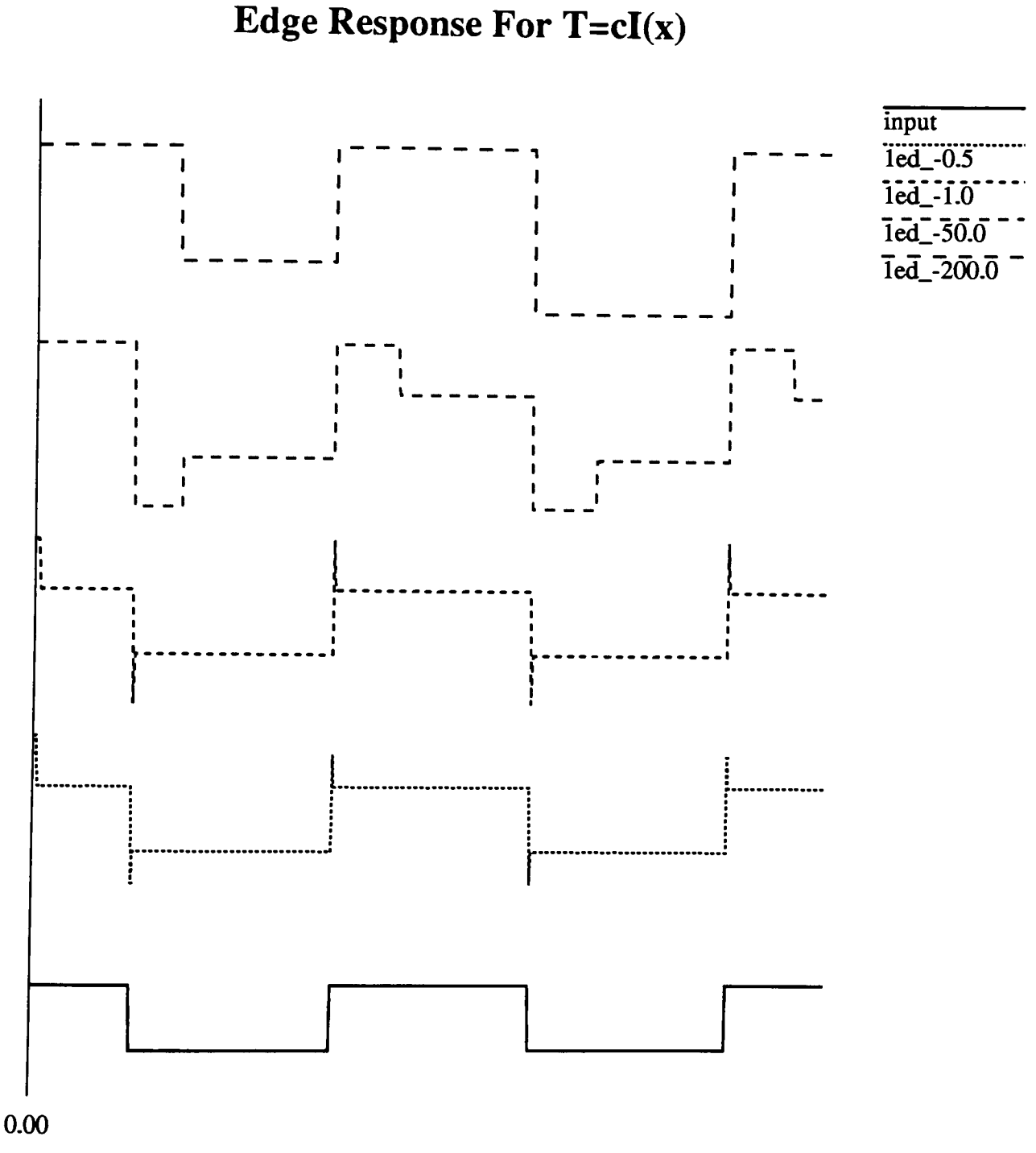

Figure 4.8: Edge Response of ED with T = cI(x); for c = -0.5, c=-1.0, c= -50, c=-200

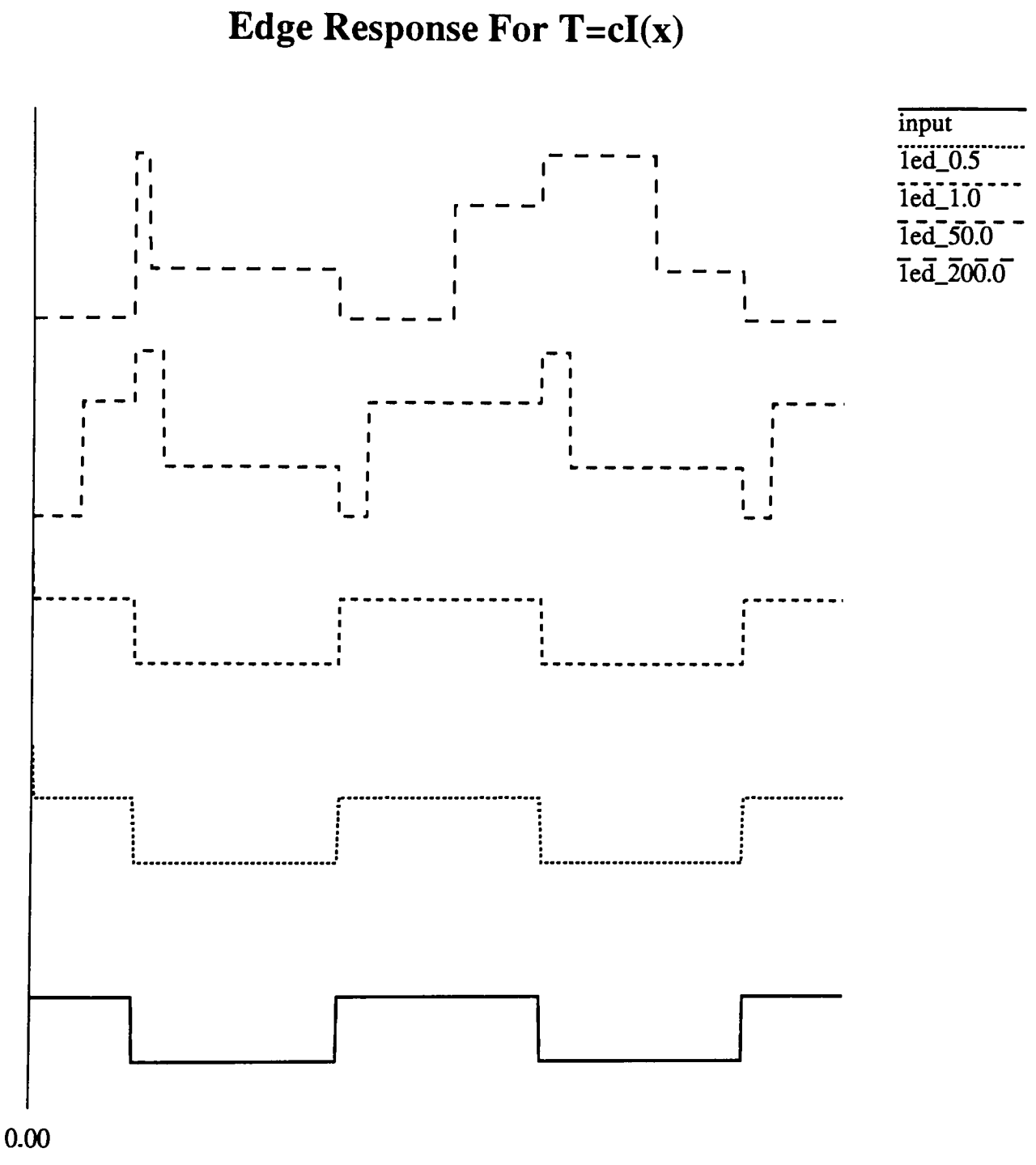

Figure 4.9: Edge Response of ED with T = cI(x); for c = 0.5, c=1.0, c= 50, c=200

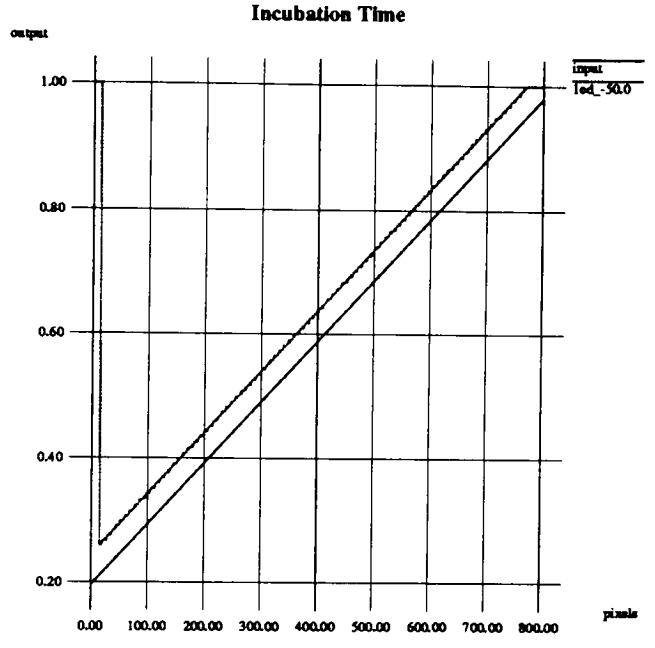

Figure 4.10: Incubation time for threshold modulation = cI(x); c= -50

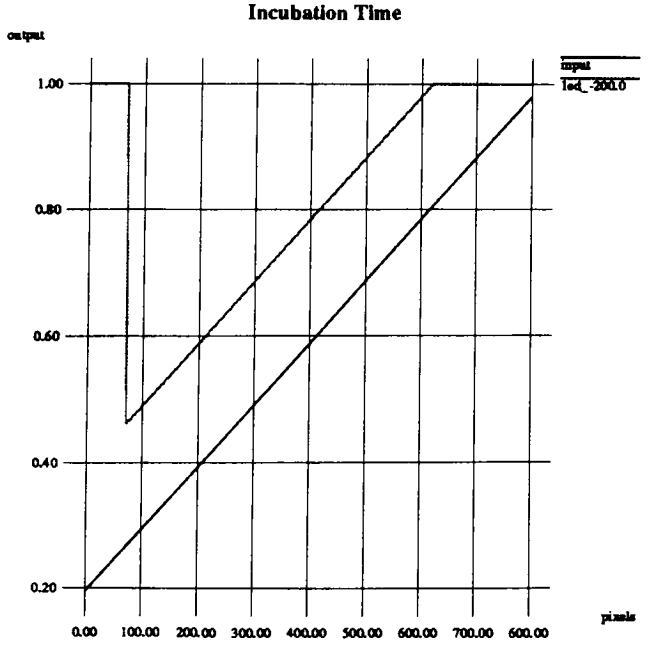

Figure 4.11: Incubation time for threshold modulation = cI(x); c= -200

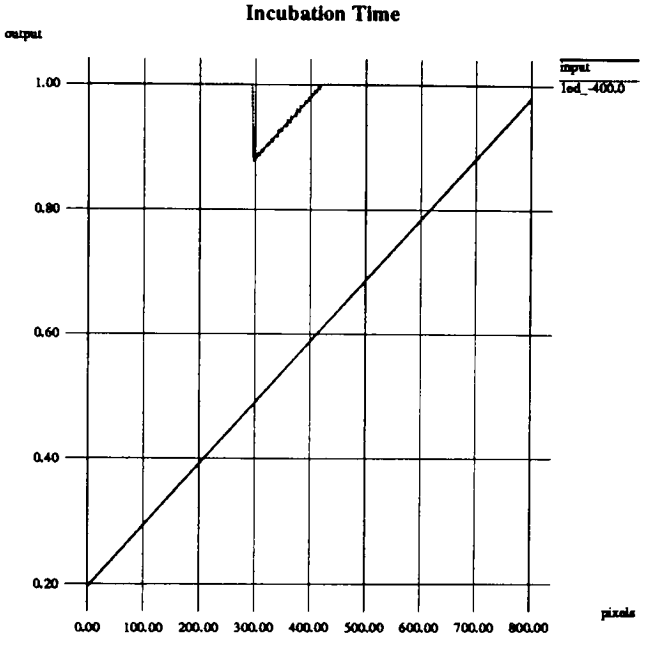

Figure 4.12: Incubation time for threshold modulation = cI(x); c= -400

The first observations of threshold modulation in 1-D ED are:

1. the edge enhancement is asymmetric,
2. the output for a linear input is shifted, according to the value of the parameter c,
3. a different type of incubation is observed for a block input, and
4. the threshold variation drastically changes the well known behavior of the standard 1-D ED.

4.2 PDM with additional phase modulation as a model for ED

The fact that the edge enhancement can be controlled by substituting the fixed threshold in ED with an input-dependent one indicates that an additional phase modulation in PDM should produce the same effect.

The proposed phase modulation introduced in the PDM can be described by generalizing eq. 3.5 to the following :

$$C(x) = cos[\frac{2\pi}{\lambda I_0}(\int_0^x I(u)du + \phi_1(x) + \phi_0)] \tag{4.1}$$

where $\phi(x)$ is an additional phase that can be any function of the input. It is possible to include all the position dependent-information into the frequency term, because of the relation between frequency and phase :

$$\omega(x) = \frac{\partial \phi}{\partial x}(x) \tag{4.2}$$

or

$$\int_0^x \omega(x)dx + \phi(0) = \phi(x). \tag{4.3}$$

Therefore the phase modulation can be interpreted as a frequency modulation by rewriting eq.(4.1) to obtain:

$$C(x) = cos[\frac{2\pi}{\lambda I_0}\{\int_0^x (I(u) + \frac{\partial \phi_1}{\partial u}(u))du + \phi_1(0) + \phi_0\}]. \tag{4.4}$$

By comparing Eq.(4.4) with the standard expression (3.5), the new expression implies that it is possible to describe the edge-enhanced error diffusion as a two-step process in which the object $I(n)$ is first changed to $I(n) - \frac{\partial T}{\partial n}(n)$ (where T is the threshold) followed by standard error diffusion.

4.3 Characterization of ED with threshold modulation

If PDM combined with phase modulation is an adequate model for ED with threshold modulation, the output of ED with $T(x) = cI(x)$ should correspond to the output of standard ED for an input $I(x) - c\frac{\partial I(x)}{\partial x}$. The observations of the effect of threshold modulation in ED (summarized in previous section) do not violate these statements, but rather are reinterpreted.

1. The asymmetry of edge enhancement at the edges corresponds to the unidirectional derivative at such a transition.

2. Moreover, the sign of the constant c determines whether there is an overshoot or an undershoot. If c is negative the derivative is added to the input function which gives overshoot at a transition from dark to light. The height of the overshoot corresponds to the value of the derivative, if the value $I(x) - c\frac{\partial I(x)}{\partial x}$ is limited to the normal range $[0, I_0]$. This statement is absolutely confirmed by the average response of the linear input which is simply shifted by a constant, being the derivative of this function. As mentioned in section 3, ED will compensate for out-of-range values by saturating until the overall integrated value is corrected. Although the next input value I(x) may be a perfectly legal value in the allowed range, threshold modulation in ED treats the input identically to standard ED with $I(x) - c\frac{\partial I(x)}{\partial x}$. Therefore a so-called *hidden saturation* occurs for large $\frac{\partial I(x)}{\partial x}$ or for large $|c|$.

3. The incubation time at the left side of the graphs, is due to the fact that the range of starting error over which is averaged is adapted for I(x) but not for $I(x) - c\frac{\partial I(x)}{\partial x}$. Instead of producing the first pulse according to equation (3.18), ED will respond

again to input values as soon as:

$$T(n) \leq \sum_{k=0}^{n} I(k) + E(-1). \tag{4.5}$$

4.4 The variable threshold as a convolution mask

The previous predictions can be confirmed if identical ED outputs are obtained by taking the following separate paths: ED executed with fixed threshold on an enhanced image, and ED executed on the original image but using a suitable variable threshold. Because ED applies to sampled data, the relationship between the threshold and the enhancing term has to be calculated carefully in order to collect the same information.

4.4.1 First derivative enhancement

If the threshold in ED is proportional to the input, no forward information is introduced to the image and therefore the derivative used to compute the convolution mask has to be calculated between points n and $n-1$. For the case of the threshold being proportional to the input, the results are:

$$\begin{aligned} \phi_1(x) &= -cI(x) \\ \frac{\partial \phi_1}{\partial x}(x) &= -c\frac{\partial I}{\partial x}(x) \\ &=> -c[I(n) - I(n-1)]. \end{aligned}$$

The statement of equivalent processing has been investigated by averaging the output of ED over starting error. The starting error range has been adapted according to equation 0.1 for the threshold variation, while it was adapted according to 3.18 for the equivalent

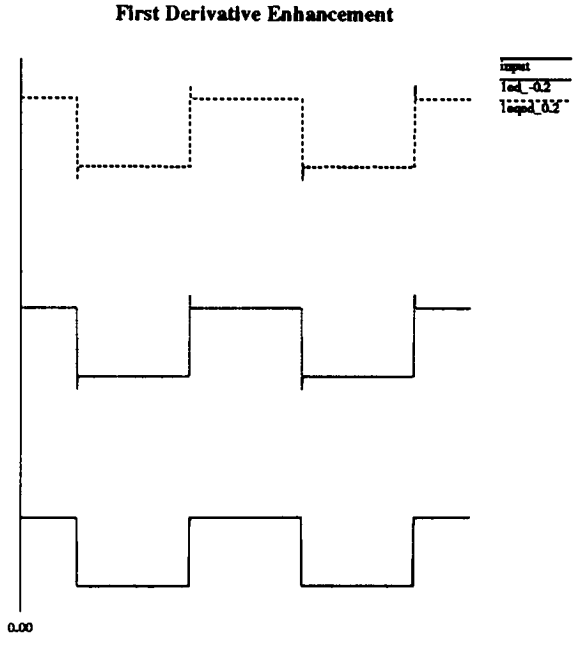

Figure 4.13: ED with threshold proportional to input and ED with equivalent mask (c= -0.2)

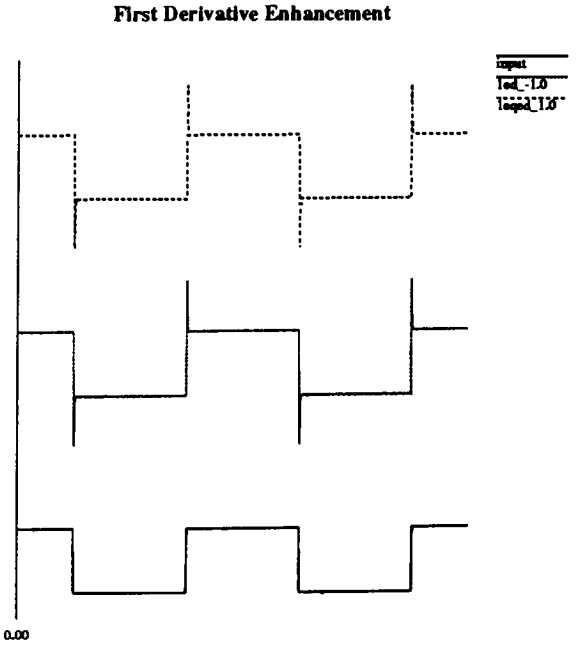

Figure 4.14: ED with threshold proportional to input and ED with equivalent mask (c=

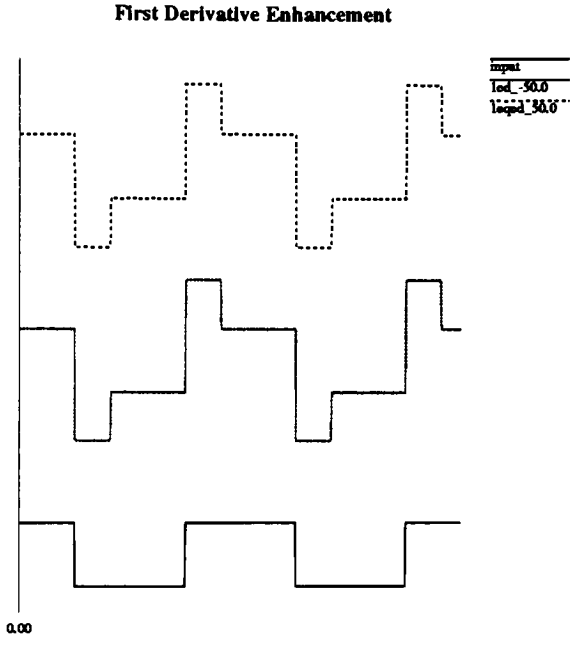

Figure 4.15: ED with threshold proportional to input and ED with equivalent mask (c= -50.0)

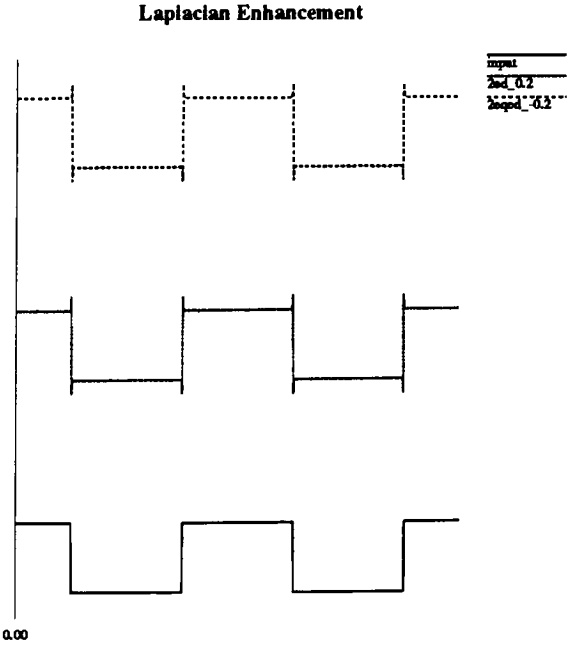

Figure 4.16: Laplacian enhancement, obtained with and without mask (c= 0.2)

Figure 4.17: Threshold modulation proportional to the input (c=-2)

Figure 4.18: Standard error diffusion preceded by filtering by adding first derivative(c=-2)

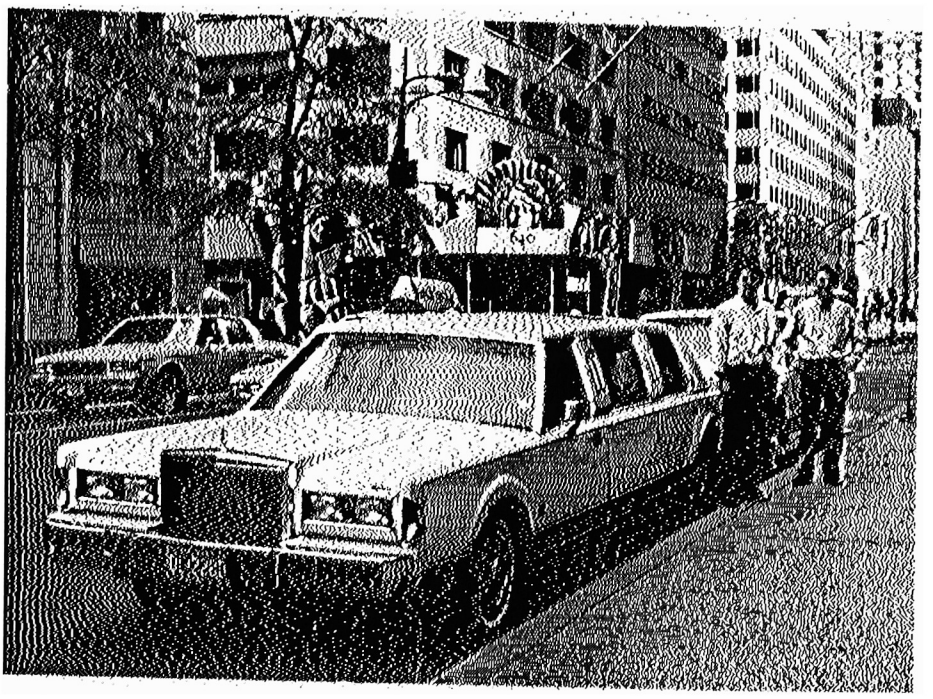

Figure 4.19: Threshold modulation proportional to the input (c=-4)

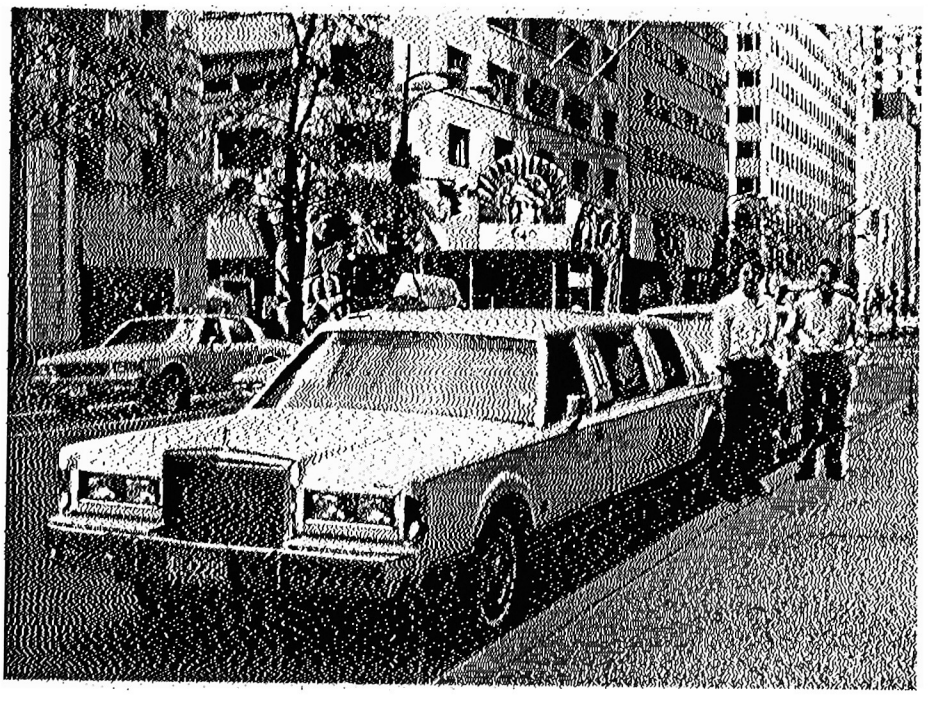

Figure 4.20: Standard error diffusion preceded by filtering by adding first derivative(c=-4)

Figure 4.21: Threshold modulation proportional to the input (c=-40)

Figure 4.22: Standard error diffusion preceeded by filtering by adding first derivative(c=-40)

process. Figure 0.1 shows the case for a threshold proportional to the input. The profile at the bottom shows the input function with the result of the edge-enhanced ED algorithm at the top of the graph. The profile in the middle shows the result of applying the convolution mask given in Table 1 to the image before using the standard ED algorithm. Figures 0.2, 0.3 show the corresponding cases for respective values $c = -1.0, c = -50$. For this large enhancement, saturation can be seen at upward and downward transitions. The incubation time has disappeared, which affirms the accuracy of its interpretation. The same algorithms have been applied to a scanned image as shown in Figures 0.5 and 0.6, 0.7 and 0.8, 0.9 and 0.10.

4.4.2 Second derivative enhancement

The model correctly predicts the equivalent mask for error diffusion with threshold modulation. The validity will be confirmed if the model can predict the appropriate threshold variation for an arbitrary sharpening mask. A very common mask is the Laplacian:

| -c | 2c + 1 | -c |

for which the edge enhancement is symmetric, in contrast to threshold modulation with $T(x) = cI(x)$. Because the Laplacian mask is the digital version of subtracting the second derivative from the input, the threshold modulation must be proportional to the first derivative of the input function. The calculation of the discrete first derivative is done with the perspective of a Laplacian mask at the output. Because the kernel of the Laplacian mask has a symmetric width of 3 pixels, it is necessary to calculate a forward derivative.

$$\begin{aligned} \phi_1(x) &= -c\frac{\partial I}{\partial x}(x) \\ &=> -c[I(n+1) - I(n)] \end{aligned}$$

TABLE 1	ED input	ED threshold
general	$I(x) + \frac{\partial \phi_1}{\partial x}(x)$	$-\phi_1(0) - \phi_0$
	$I(x)$	$-\phi_1(x) - \phi_0$
first derivative enhancement	$\boxed{0 \mid 1-c \mid c} * I(n)$	$cI(0) - \phi_0$
	$I(n)$	$cI(n) - \phi_0$
Laplacian enhancement	$\boxed{-c \mid 2c+1 \mid -c} * I(n)$	$\boxed{0 \mid -c \mid c} * I(n)\|_{n=0} - \phi_0$
	$I(n)$	$\boxed{0 \mid -c \mid c} * I(n) - \phi_0$

Figure 4.23: Convolution masks, equivalent to threshold modulation for ED processing

$$\begin{aligned} \frac{\partial \phi_1}{\partial x}(x) &= -c\frac{\partial^2 I}{\partial x^2}(x) \\ &= -c[\frac{\partial I}{\partial x}(x)|_{x+\Delta x} - \frac{\partial I}{\partial x}(x)|_x] \\ &=> -c[I(n+1) - 2I(n) + I(n-1)]. \end{aligned}$$

The convolution masks to be applied on the input are given in Figure 0.11, for the same cases as indicated above.

Corresponding to averaging of ED for first-derivative enhancement, Figures 0.4, 0.12 and 0.13 show the situation for the ED (top) with threshold being proportional to the first

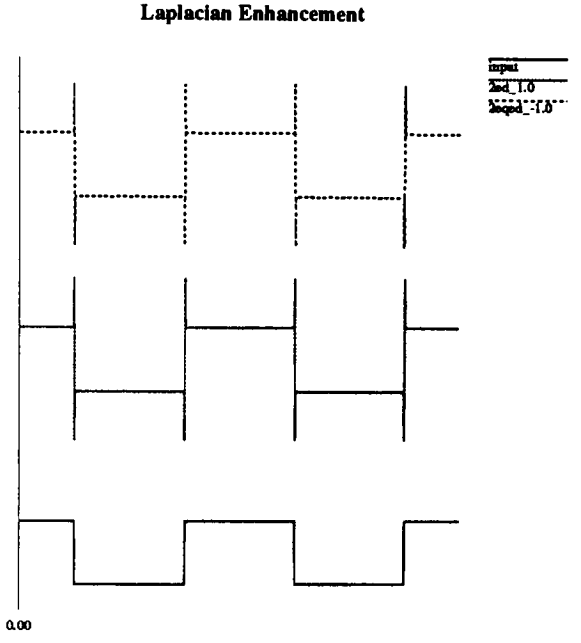

Figure 4.24: Laplacian enhancement , obtained with and without mask (c= 1.0)

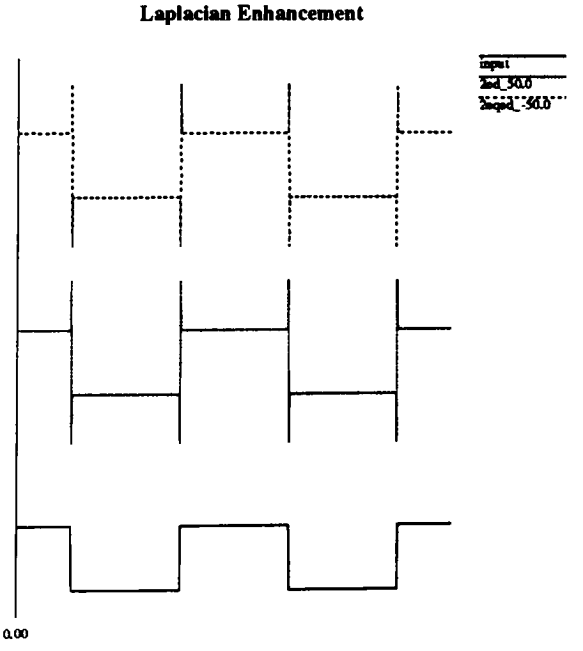

Figure 4.25: Laplacian enhancement, obtained with and without mask (c= 50.0)

Figure 4.26: Threshold modulation proportional to the derivative of the input (c=2)

Figure 4.27: Standard error diffusion preceeded by filtering by a Laplacian mask (c=2)

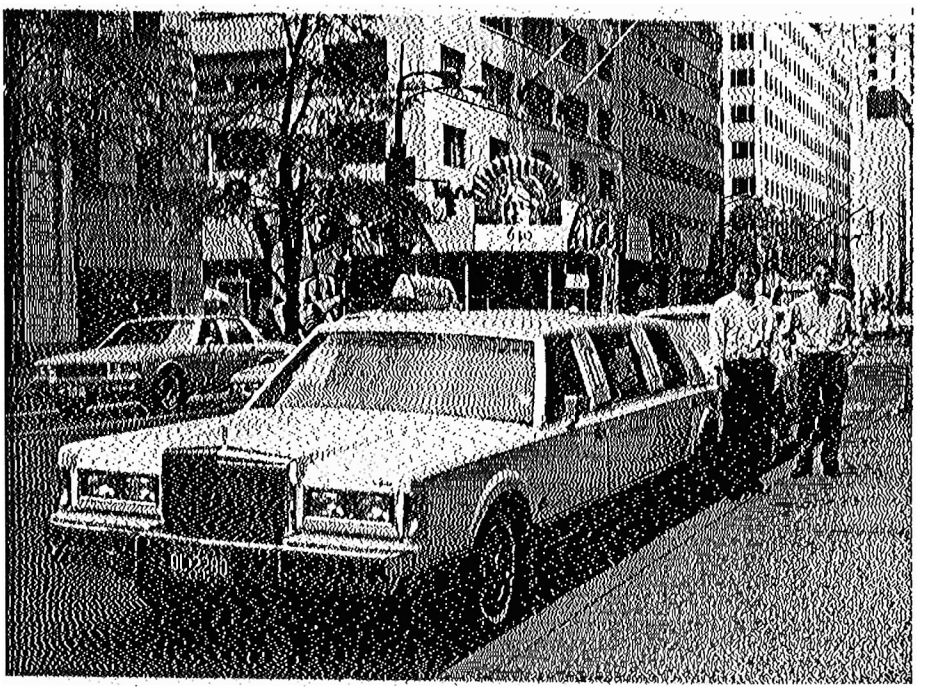

Figure 4.28: Threshold modulation proportional to the derivative of the input (c=4)

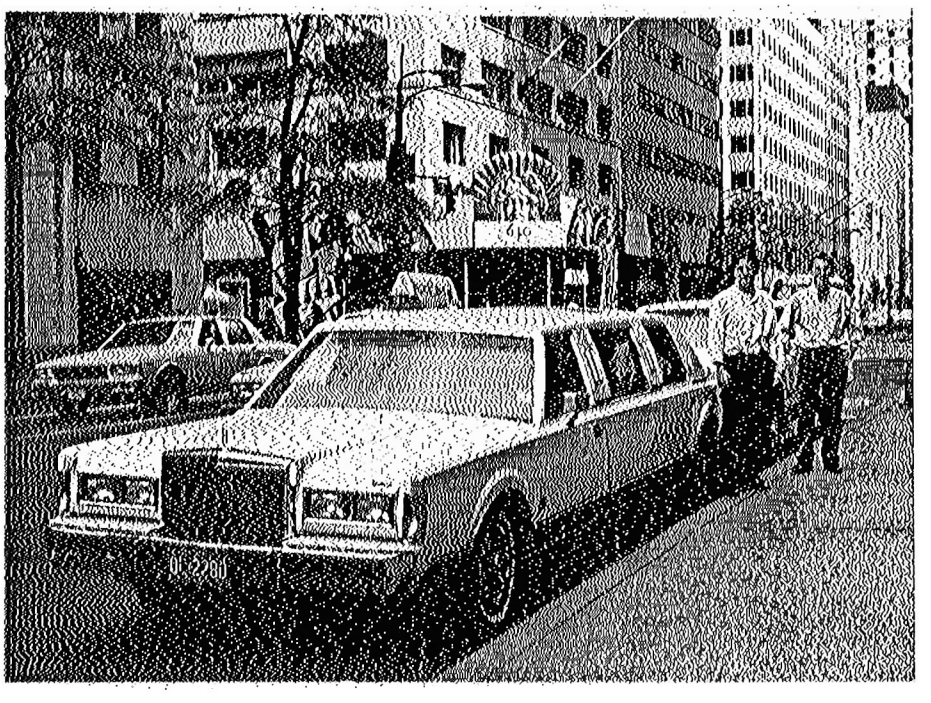

Figure 4.29: Standard error diffusion preceeded by filtering by a Laplacian mask (c=4)

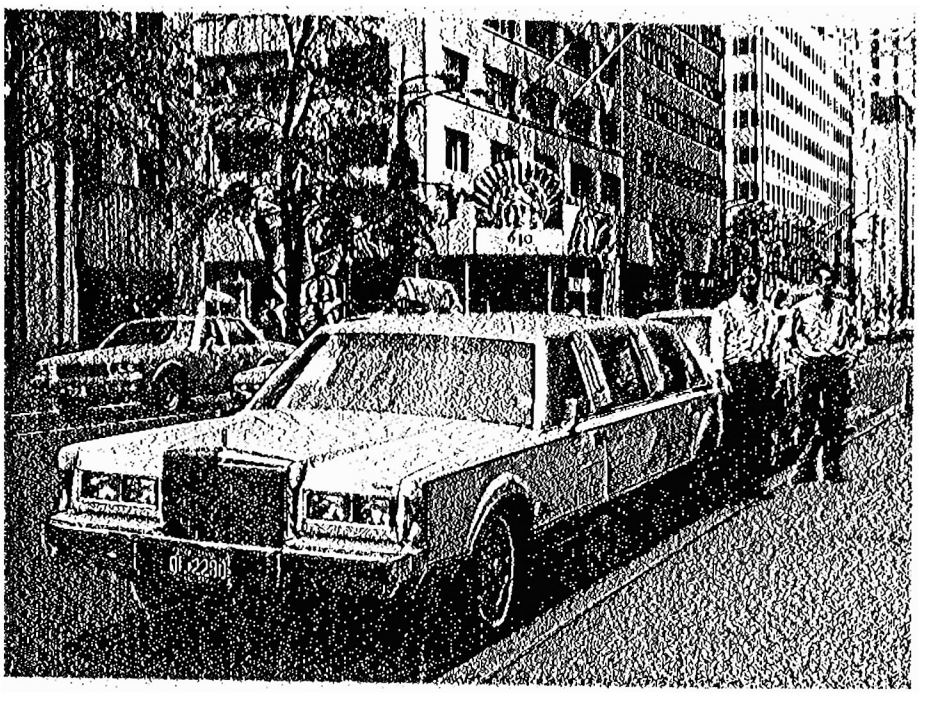

Figure 4.30: Threshold modulation proportional to the derivative of the input (c=40)

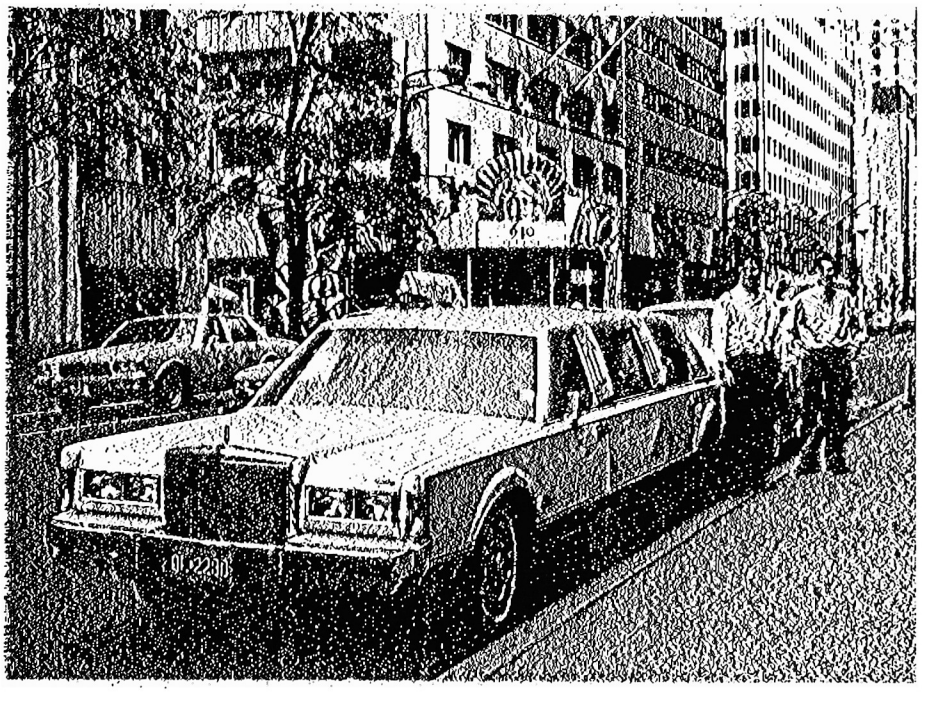

Figure 4.31: Standard error diffusion preceeded by filtering by a Laplacian mask (c=40)

Figure 4.32: Threshold modulation proportional to the derivative of the input (c=-50)

Figure 4.33: Threshold modulation proportional to the input (c = 50)

derivative of the input (bottom), giving rise to the more common Laplacian convolution (middle). Again there is agreement between the proposed equivalent processing types. For this type of enhancement, no extended saturation is found even for large c. This statement is clearely confirmed by the result of applying the two types of threshold modulation for the same large parameter $|c|$ (Figures 4.32, and 4.33). Verification of the equivalent processing types for the symmetric enhancement can be done by judging the similarity of the images in Figures 4.26 and 4.27, 4.28 and 4.29, 4.30 and 4.31.

4.4.3 Noise evaluation for threshold variation

Because the character of the threshold modulation has been predicted by the PDM model, it should also be possible to investigate the way threshold modulation handles noise. Threshold modulation proportional to the input has previously been described as very unsensitive to noise when ED is applied in 2D[EK91] . The averaging over the starting error, as when calculating the edge response for ED, gives the probability for a binary output to occur. In the 1D case, we expect that an input distorted by noise

$$I_{noise}(n) = I(n) + N(n) \tag{4.6}$$

will have an output probability $\tilde{O}(n)$ of

$$\tilde{O}(n) = I(n) + N(n) - c(I(n) - I(n-1)) - c(N(n) - N(n-1)) \tag{4.7}$$

if the threshold equals $T = cI(n)$. This probability holds only for the output $\tilde{0}(n)$ in the regular range of $[0, 255]$. The additional term added to the output probability equals $N(n) - c(N(n) - N(n-1))$. Depending on the mean and the frequency characteristics of the noise the extra term may affect the output differently. However the noise term may have little influence on precipitating or delaying the incubation period when the output is

in saturation mode as long as the integral of the additional term equals zero. In this case it will not contribute to the unloading of the error. In the case of Laplacian enhancement, we obtain the sum of the input itself and frequency term originating from the overall input. It is obvious that if noise is present, it will contribute to this output probability. Examples of images disturbed with noise and their originals, processed by error diffusion with several threshold modulations are shown below (Figures 4.34, 4.35, 4.36).

4.5 Numerical identities

Whereas the PDM model has served as a basis to derive equivalent filtering masks to describe the enhancement obtained by threshold modulation, it is also possible to demonstrate numerically that these processing methods are identical when the appropriate constants are used for the starting error and/or threshold. The proofs for both first and second derivative can be found in appendix A (section 1 and 2).

In addition, a general threshold modulation can be specified for any linear filter $\triangle(n)$ as proven in section 3 of Appendix A and also mentioned in the table (Figure 4.37). These results confirm the validity of the PDM model for ED in a very convincing way. The derivative of the threshold modulation for a general linear filter would be identical to calculating the corresponding phase modulation for a known frequency modulation with continuous input $I(x) + \triangle(x)$ and constant phase. Using the carrier 2.10, with the filtered input results in

$$C(x) = cos[\frac{2\pi}{\lambda I_0}(\int_0^x [I(u) + \triangle(u)]du + \phi_0)]. \tag{4.8}$$

It is obvious that if we isolate a frequency term corresponding to the original input, the remaining phase function will be variable and equal:

$$\phi(x) = \int_0^x \triangle(u)du + \phi_0 \tag{4.9}$$

Figure 4.34: ED processed on disturbed image with additive gaussian noise (zero mean, std. 30 for a range of $[0, 255]$)

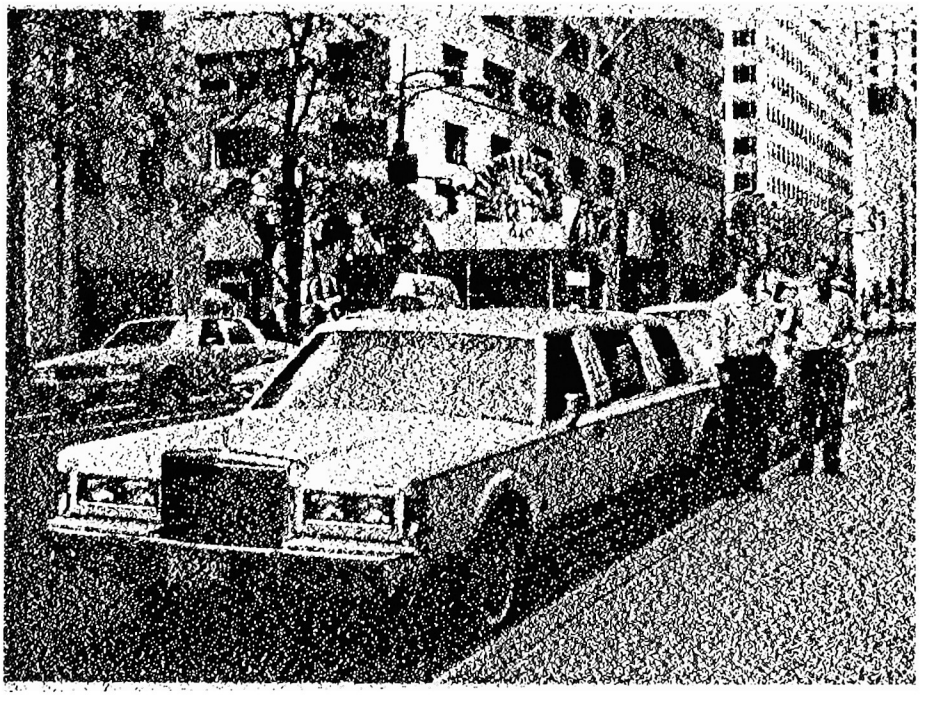

Figure 4.35: ED with threshold modulation T = cI(x) on noisy image (c=-10)

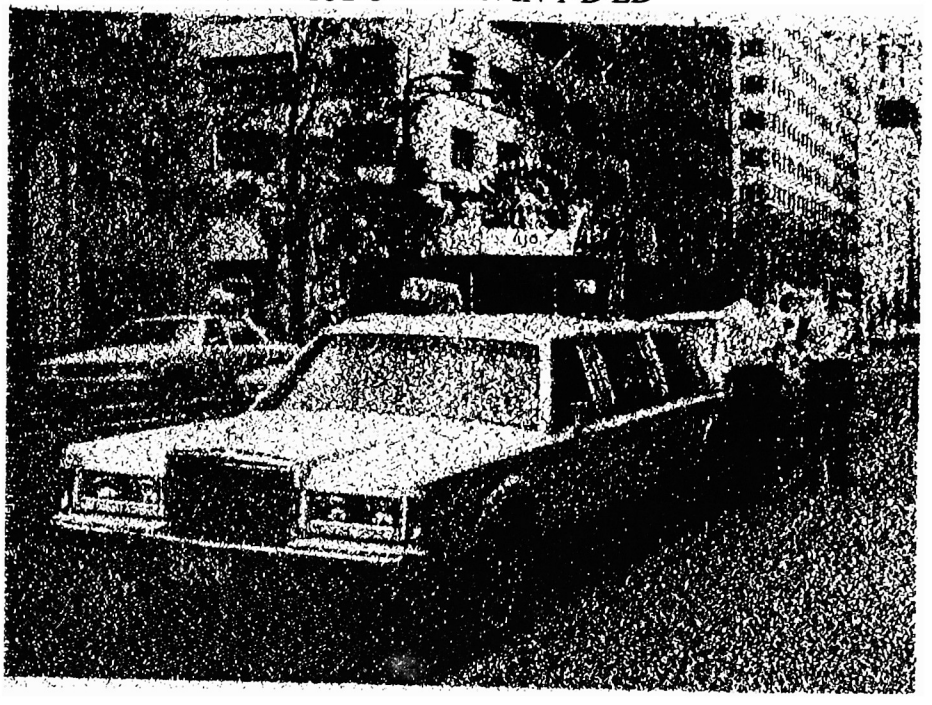

Figure 4.36: ED with threshold modulation $T = c\frac{\partial I(x)}{\partial x}$ on noisy image (c = 10)

TABLE 2	ED input	ED threshold	ED starting error
general	$I(n) + \triangle(n)$	T	$E(-1)$
	$I(n)$	$T - \sum_{k=0}^{n} \triangle(k)$	$E(-1)$
first derivative enhancement	$\boxed{0 \mid 1-c \mid c} * I(n)$	T	$E(-1)$
	$I(n)$	$cI(n)$	$E(-1) + cI(-1) - T$
Laplacian enhancement	$\boxed{-c \mid 2c+1 \mid -c} * I(n)$	T	$E(-1)$
	$I(n)$	$c[I(n+1) - I(n)]$	$E(-1) + c[I(0) - I(-1)] - T$

Figure 4.37: Convolution masks, identical to threshold modulation for ED processing

This corresponds completely to the general threshold modulation for the digital filter.

For any threshold modulation, a corresponding analytical filter can be found (see proof 4 in appendix)

4.5.1 Lowpass filter as an example

The lowpass filter which averages over three pixels, can be written in the format of previous derivation as

$$I(n) + \triangle(n) = \frac{I(n+1) + I(n) + I(n-1)}{3} \tag{4.10}$$

with

$$\triangle(n) = \frac{I(n+1) - 2I(n) + I(n-1)}{3}. \tag{4.11}$$

Consequently the equivalent threshold modulation for an error diffusion on the original input $I(n)$, would be :

$$\begin{aligned} T(n) &= \sum_{k=0}^{n} \triangle(k) \\ &= \sum_{k=0}^{n} \frac{I(k+1) - 2I(k) + I(k+1)}{3} \\ &= \sum_{l=1}^{n+1} \frac{I(l)}{3} - \sum_{k=0}^{n} \frac{2I(k)}{3} + \sum_{m=-1}^{n-1} \frac{I(m)}{3}. \end{aligned} \tag{4.12}$$

The terms with indices $1 \leq i \leq n-1$ cancel so that the expression for the treshold modulation reduces to:

$$\begin{aligned} T(n) &= \frac{I(n+1)}{3} + \frac{I(n)}{3} - \frac{2I(n)}{3} - \frac{2I(0)}{3} + \frac{I(-1)}{3} + \frac{I(0)}{3} \\ &= [\frac{I(n+1) - I(n)}{3}] + [\frac{I(-1) - I(0)}{3}] \end{aligned} \tag{4.13}$$

Chapter 5

Results in 2D

Whereas one-dimensional error diffusion is nicely modeled by PDM, the two-dimensional Floyd-Steinberg algorithm cannot be described by the extension of the PDM to two dimensions. This problem has been extensively discussed in Chapter 2. The main reason for this discrepancy, is that whereas the integral in PDM contains the exact same information as the history dependent error E(n) in error diffusion, the error is distributed to four neighbors so that the integrated information is spread over four points.

Although the analytical model is not valid in 2-D, some characteristics can be explained by assuming that the threshold keeps the same function. Because exact analysis of threshold modulation requires a completely new model, the discussion will be restricted to the similarities between the results obtained in one and two dimensions. The similarities will be illustrated by images.

- As described in chapter 2, the binary images show unidirectional edge enhancement for threshold modulation $T(x) = cI(x)$, which indicates a first derivative enhancement. The values of c correspond to the equivalent type of shadowing in 1-D ED with threshold variation. The opposite shadowing occurs when the direction of processing

is reversed, while a different result is obtained if we take the opposite negative value of c.

In both Figures 5.1 and 5.2 a threshold proportional to the input with parameter K = 10 is used (c = -9), but with a different sequence of processing. In Figure 5.1, the image is processed according to the standard order from the left to the right hand side, and from top to bottom. The other image 5.2 is processed by ED right to left and bottom to top. The different appearance is that although the same direction of overshoot is used, the direction in which the saturation is extended is opposite. The corresponding negative parameter ($K = -8$; $c = 9$) used in Figure 5.3, subtracts the derivative, and saturation zones are created at different positions. This indicates again that the effect of adding the derivative after the point of processing is present.

- The blurring effect which is present in two dimensions (for $K < 1$, and small) is hardly visible in one dimension due to the fact that only a fraction of the derivative is added or subtracted because of the error distribution. For different values of the error distribution, but the same threshold modulation, the edge enhancement is rendered differently (see Figures 5.4 and 5.5).

- The fact that threshold modulation proportional to the input is stable for noisy inputs, is in accordance with the statement made in the noise evaluation in one dimension. Illustrations are given in Figures 5.6 and 5.7.

Figure 5.1: Standard ED with T(x) = -9 I(x), processed from left to right and top to bottom

Figure 5.2: Standard ED with T(x) = -9 I(x), processed from right to left and bottom to top

Figure 5.3: Standard ED with T(x) = 8 I(x), processed from left to right and top to bottom

Figure 5.4: ED with T(x) = -9 I(x), weights are $\frac{7}{16}\frac{1}{16}, \frac{5}{16}, \frac{3}{16}$

Figure 5.5: ED with T(x) = -9 I(x), weights are $\frac{1}{4}, \frac{1}{4}, \frac{1}{4}, \frac{1}{4}$

Figure 5.6: ED on noisy image (gaussian; zero mean; std = 30)

Figure 5.7: ED with T(x) = - I(x), on noisy image (gaussian; zero mean; std = 30)

Conclusions

We have explained the edge enhancement obtained by an input dependent threshold in 1-D ED by using an analytical model for ED. The resulting sharpening can be accurately predicted and controlled. It is possible to produce the equivalent result of inserting a preprocessed image in ED or by processing the original image through ED with variable threshold. The output obtained by introducing a threshold proportional to the derivative of order n of the input is equivalent to adding the (n + 1)-th order derivative to the original input weighted with the same proportionality constant. This might be advantageous for computer implementations to reduce complexity and to increase speed. By using a threshold proportional to the input versus adding a derivative to the image, we avoid the use of a convolution mask. Hereby we showed also that a threshold proportional to the input shows only one-directional edge enhancement because of its first-order character. Although the analytical model is not valid in 2-D, we have confidence that the parameters have the same function as in one dimension, and therefore some characteristics can be explained by similar reasoning.

Appendix A

numerical proofs

A.1 Proof1: Equivalent first derivative enhancement

The mathematical description of ED by the three equations (3.12), (3.13) and (3.14) can be combined, and by recursion one general expression can be derived:

$$B(n) = step[I(n) + \sum_{k=0}^{n-1}(I(k) - B(k)) + E(-1) - T], \qquad \text{(A.1)}$$

where $E(-1)$ is the starting error added to the input of the first pixel indexed by $k = 0$. If the input is first convolved by adding the first derivative enhancement filter derived in previous section, the binary output will be:

$$\begin{aligned} B(n) &= step\{(1-c)I(n) + cI(n-1) + \sum_{k=0}^{n-1}[(1-c)I(k) + cI(k) - B(k)] \\ &\quad + E(-1) - T\}. \end{aligned} \qquad \text{(A.2)}$$

By separating the terms occuring in equation A.1, an additional term is isolated (bold font):

$$B(n) = step\{I(n) + \sum_{k=0}^{n-1}(I(k) - B(k)) + E(-1) - T$$

$$-\mathbf{c[I(n) - I(n-1)]} + \sum_{\mathbf{k=0}}^{\mathbf{n-1}} \mathbf{c[I(k-1) - I(k)]}\} \quad \text{(A.3)}$$

The additional term can be simplified as all the terms in the sum cancel except for those with index $k = 0$ and $k = n - 1$, only remaining:

$$-\mathbf{c[I(n) - I(n-1)]} + \mathbf{c[I(-1) - I(n-1)]} = \mathbf{cI(-1) - cI(n)} \quad \text{(A.4)}$$

If we substitute these two terms in equationA.3, we can distribute them arbitrarely between starting error and threshold:

$$B(n) = step\{I(n) + \sum_{k=0}^{n-1}(I(k) - B(k)) + [E(-1) + cI(-1) - T] - [cI(n)]. \quad \text{(A.5)}$$

Since equation A.2 and A.5 are identical expressions it is proven that:

The result of applying error diffusion with a varying threshold $T(n) = cI(n)$ and starting error$E(-1) + cI(-1) - T$ is identical to applying standard error diffusion with fixed threshold T and starting error $E(-1)$ on a preprocessed image, which was convolved with the filter $(c, 1-c, 0)$ with the unknown value $I(-1)$ used as in the expression for the starting error in the first method.

A.2 Proof2: Equivalent Laplacian enhancement

A similar path can be taken to proof the equivalent Laplacian enhancements in ED. If we insert an image processed by convolution with the mask $(-c, 2c+1, c)$ in the standard error diffusion expression A.1, the binary output will be:

$$\begin{aligned} B(n) \;=\; & step\{-cI(n-1) + (2c+1)I(n) - cI(n+1) \\ & + \sum_{k=0}^{n-1}[-cI(k-1) + (2c+1)I(k) - cI(k+1) - B(k)] \\ & + E(-1) - T\} \end{aligned} \quad \text{(A.6)}$$

Sorting the familiar terms results in:

$$\begin{aligned} B(n) &= step\{I(n) + \sum_{k=0}^{n-1}[I(k) - B(k)] + E(-1) - T \\ &\quad \mathbf{-cI(n-1) + 2cI(n) - cI(n+1)} \\ &\quad \mathbf{+ \sum_{k=0}^{n-1}[-cI(k-1) + 2cI(k) - cI(k+1)]}\}. \end{aligned} \tag{A.7}$$

The bold term can be rewritten by using new indices in the summation as:

$$\begin{aligned} &\mathbf{-cI(n-1) + 2cI(n) - cI(n+1)} \\ &\mathbf{- \sum_{l=-1}^{n-2} -cI(l) + \sum_{k=0}^{n-1} 2cI(k) - \sum_{m=1}^{n} cI(m)} \\ &\qquad = \mathbf{-cI(n-1) + 2cI(n) - cI(n+1)} \\ &\qquad\quad \mathbf{-cI(-1) - cI(0) + 2cI(0)} \\ &\qquad\quad \mathbf{+2cI(n-1) - cI(n-1) - cI(n)} \\ &\qquad = \mathbf{-cI(-1) + cI(0)} \\ &\qquad\quad \mathbf{+cI(n) - cI(n+1)} \end{aligned} \tag{A.8}$$

Replacing the short expression for the bold term in equation A.7, gives the equivalent of equation A.6:

$$\begin{aligned} B(n) &= step\{I(n) + \sum_{k=0}^{n-1} I(k) + [E(-1) + c(I(0) - I(-1)) - T] \\ &\quad -[c(I(n+1) - I(n))]\}. \end{aligned} \tag{A.9}$$

Since both expressions A.6 and A.9 are identical, it is proven that:

applying standard error diffusion with starting error $E(-1)$ and threshold T on an image processed by a Laplacian filter $(-c, 2c+1, -c)$, is identical to applying error diffusion with varying threshold $T(n) = c[I(n+1) - I(n)]$ on the original image, using a starting error $E(-1) + c[I(0) - I(-1)] - T$.

A.3 Proof3: Equivalent threshold modulation for linear filtering

For any linear digital filter, the following statement in 1-D will be proven:

Applying standard error diffusion with fixed threshold T on $I(n) + \triangle(n)$, is identical to applying error diffusion on $I(n)$ with varying threshold $T(n) = T - \sum_{k=0}^{n} \triangle(k)$.

Using the filtered input $I(n) + \triangle(n)$ in the general expression A.1 for the binary output of error diffusion gives:

$$B(n) = step[I(n) + \triangle(n) + \sum_{k=0}^{n-1}(I(k) + \triangle(k) - B(k)) + E(-1) - T], \quad \text{(A.10)}$$

where $E(-1)$ is the starting error added to the input of the first pixel indexed by $k = 0$. Reordening the terms, isolates the input of an original image $I(n)$ to an error diffusion with varying threshold:

$$\begin{aligned} B(n) &= step\{I(n) + \sum_{k=0}^{n-1}(I(k) - B(k)) \\ &\quad + E(-1) - [T - \sum_{k=0}^{n-1} \triangle(k) - \triangle(n)] \\ &= step\{I(n) + \sum_{k=0}^{n-1}(I(k) - B(k)) \\ &\quad + E(-1) - (T - \sum_{k=0}^{n} \triangle(k)) \end{aligned} \quad \text{(A.11)}$$

A.4 Proof4: Equivalent linear filtering for threshold modulation

For any threshold modulation $T + T(n)$ in ED, a digital linear filter can be found which will render an equivalent image when after applying the filter the standard error diffusion with fixed threshold is used for binarization. The filter is given by $\triangle(n) = -(T(n) - T(n-1))$, and when applied on an image $I(n)$, the result is $I(n) + \triangle(n)$. The threshold $T(-1)$ is considered zero.

If a threshold variation $T + T(n)$ would correspond do a linear filter $\triangle(n)$, the threshold variation needs to obey the statement in proof3.

$$T + T(n) = T - \sum_{k=0}^{n} \triangle(k)$$

$$T(n) = -\sum_{k=0}^{n} \triangle(k) \tag{A.12}$$

Since the expression is true for each n, it is possible to derive recursively the expression for $\triangle(n)$.

$$\triangle(\mathbf{n}) = -(\mathbf{T(n)} - \mathbf{T(n-1)}) \tag{A.13}$$

part1 of proof: The expression A.13 is true for n = 0

If equation A.12 is used with $n = 0$,

$$T(n) = -\triangle(0) \tag{A.14}$$

the general statement is fulfilled for $n = 0$:

$$\triangle(0) = -(T(0) - T(-1)) \tag{A.15}$$

if $T(-1)$ is considered to be zero. therefore we proved that **the expression A.13 is true for $n = 0$, if $T(-1) = 0$.**

part2 of proof: If the expression A.13 is true for all $n < k$ it is true for $n = k$

Starting with the general equation A.12 for $n = k$

$$\begin{aligned} T(k) &= -\sum_{l=0}^{k} \triangle(l) \\ &= -\triangle(k) - \sum_{l=0}^{k-1} \triangle(l) \end{aligned}$$

and using the expression A.13 for the indices smaller than k gives:

$$\begin{aligned} T(k) &= -\triangle(k) + \sum_{l=0}^{k-1}[T(l) - T(l-1)] \\ &= -\triangle(k) + \sum_{l=0}^{k-1} T(l) - \sum_{m=-1}^{k-2} T(m) \\ &= -\triangle(k) + T(k-1) - T(-1). \end{aligned} \tag{A.16}$$

Therefore the general statement

$$\triangle(k) = -[T(k) - T(k-1)] \tag{A.17}$$

is proven for k if $T(-1) = 0$, which is the same condition for part1.

Bibliography

[AL76] J.P. Allebach and B. Liu. Random quasiperiodic halftone process. *Journal of the Optical Society of America*, 66(9):909–917, 1976.

[AL77] J.P. Allebach and B. Liu. Analysis of halftone dot profile and aliasing in the discrete binary representation of images. *Journal of the Optical Society of America*, 67(9):1147–1154, 1977.

[Bar88] E. Barnard. Optimal error diffusion for computer-generated holograms. *Journal of the Optical Society of America*, 5(11):1803–1817, 1988.

[Bay73] B.E. Bayer. An optimum method for two-level rendition of continuous-tone pictures. *International Conference on Communications*, Conference Record:26–11, 26–15, 1973.

[BEB86] M. Broja, R. Eschbach, and O. Bryngdahl. Stability of active binarization processes. *Optics Communications*, 60(6):353–358, 1986.

[BHB83] C. Billotet-Hoffmann and O. Bryngdahl. On the error diffusion technique for electronic halftoning. *Proceedings of the SID*, 42(3):253–258, 1983.

[Bry78] O. Bryngdahl. Halftone images: spatial resolution and tone reproduction. *Journal of the Optical Society of America*, 68(3):416–422,

1978.

[BWB89] M. Broja, F. Wyrowski, and O. Bryngdahl. Digital halftoning by iterative procedure. *Optics Communications*, 69(3):205–210, 1989.

[BWB90] M. Bernhardt, F. Wyrowski, and O. Bryngdahl. Coding and binarization in digital fresnel holography. *Optics Communications*, 77(1):4–8, 1990.

[Car63] J. Carson. Notes on the theory of modulation. *Proceedings of the IEEE*, (june):893–896, 1963.

[Cor70] Tom N. Cornsweet. Visual perception. *Academic Press*, 1970.

[Dim88] Anastassiou Dimitris. Neural net based digital halftoning images. *ISCAS, Espoo Finland*, june, 1988.

[dJ52] F. de Jager. Deltamodulation, a method of p.c.m. transmission using the 1-unit code. *Philips Res. Rep.*, 7:442–466, 1952.

[EH84] R. Eschbach and R. Hauck. Analytic description of the 1-d error diffusion technique for halftoning. *Optics Communications*, 52(3):165–168, 1984.

[EH85] R. Eschbach and R. Hauck. Implicit binarization procedures in 1-d. *Optics communications*, 54(2):71–74, 1985.

[EH87a] R. Eschbach and R. Hauck. A 2-d pulse density modulation by iteration for halftoning. *Optics Communications*, 62(5):300–304, 1987.

[EH87b] R. Eschbach and R. Hauck. Binarization using a two-dimensional pulse-density modulation. *Journal of the Optical Society of America*, 4(10):1873–1878, 1987.

[EK91] R. Eschbach and K.T. Knox. Error diffusion algorithm with edge enhancement. *Submitted to Journal of the Optical Society of America*, 1991.

[Esc90] R. Eschbach. Pulse-density modulation on rastered media: combining pulse-density modulation and error diffusion. *Journal of the Optical Society of America*, 7(4):708–716, 1990.

[FR76] A.J. Frank and Groff. R.H. On statistical coding of two-tone image ensembles. *Proceedings of the SID*, 17(2):102–110, 1976.

[FS76] W. Floyd and L. Steinberg. An adaptive algorithm for spatial greyscale. *Proceeding of the SID*, 17(2):75–77, 1976.

[FS86] G.S. Fawcett and G.F. Schrack. Halftoning techniques using error correction. *Proceedings of the SID*, 27(4):305–308, 1986.

[GG84] S. Geman and D. Geman. Stochastic relaxation, gibbs distributions, and the bayesian restoration of images. *IEEE Trans. on Pattern Analysis and Machine Intelligence*, PAMI-6(6):721–741, 1984.

[GS73] R.W. Gerchberg and W.O. Saxton. A practical algorithm for the determination of phase from image and diffraction plane pictures. *Optik*, 36(9):237–246, 1973.

[Hal76] J.A.G. Hale. Dot spacing modulation for the production of pseudo grey pictures. *Proceeding of the SID*, 17(2):63–74, 1976.

[HMOH89] H. Haneishi, T. Masuda, N. Ohyama, and T. Honda. Three-dimensional blood vessel reconstruction by simulated annealing. *Optics Letters*, 14(20):1095–1097, 1989.

[Hol80] T.M. Holladay. An optimum algorithm for halftone generation for displays and hard copies. *Proceedings of the SID*, 21(2):185–192, 1980.

[IY62] H. Inose and Y Yasuda. A unity bit coding method by negative feedback. *IRE Trans. on Space Electronics and Telemetry*, 8:204, 1962.

[JJN76] J.F. Jarvis, C.N. Judice, and W.H. Ninke. A survey of techniques for the display of continuous tone pictures on bilevel displays. *Computer Graphics and Image Processing*, 5:13–40, 1976.

[JR76] J.F. Jarvis and C.S. Roberts. A new technique for displaying continuous tone images on a bilevel display. *IEEE Transactions on communications*, 24:891–898, 1976.

[KMNK89] T. Kurosawa, Y. Maruyama, K. Nakazato, and H. Kotera. High speed bi-level reproduction algorithm and its lsi processor mn8361. *IEEE Int. Conf. on Image Processing*, sept 5-8, 1989.

[KMW70] R.K. Klensch, D. Meyerhofer, and J.J. Walsh. Electronically generated halftone pictures. *RCA Review*, sept:517–531, 1970.

[Kno89] K.T. Knox. Edge enhancement in error diffusion. *Paper Summaries of SPSE 1989 annual meeting*, pages 310–313, 1989.

[Knu87] Knuth. Digital halftones by dot diffusion. *ACM Transactions on Graphics*, 6(4):245–273, 1987.

[KR75] D. Kermisch and P.G. Roetling. Fourier spectrum of halftone images. *Journal of the Optical Society of America*, 65(6):716–723, 1975.

[Lim69] J.O. Limb. Design of dither waveforms for quantized visual signals. *Bell System Tech. J.*, 48:2555–2582, 1969.

[LK71] B. Lippel and M. Kurland. The effect of dither on luminance quantization of pictures. *IEEE Trans. Communication Technology*, 6:879–888, 1971.

[MBB90] R. Mrusek, M. Broja, and O. Bryngdahl. Halftoning by carrier and spectrum control. *Optics Communications*, 75(5,6):375–380, 1990.

[Mor74] T.H. Morrin. A black-white representation of a grey scale picture. *IEEE Trans. Computers*, C-23:184–186, 1974.

[Roe76a] P.G. Roetling. Halftone method with edge enhancement and moire suppression. *Journal of the Optical Society of America*, 66(10):985–989, 1976.

[Roe76b] P.G. Roetling. Visual performance and image coding. *Proceeding of the S.I.D*, 17(2):111–114, 1976.

[SAS87] M.A. Seldowitz, J.P. Allebach, and D.W. Sweeney. Synthesis of digital holograms by direct binary search. *Applied Optics*, 26(14):2788–2798, 1987.

[Sch69] Manfred R. Schroeder. Images from computers. *IEEE spectrum*, march:66–76, 1969.

[SM81] J.C. Stoffel and J.F. Moreland. A survey of electronic techniques for pictorial image reproduction. *IEEE transactions on communications*, 29(12):1898–1924, 1981.

[SM90] J. Sullivan and R. Miller. New algorithm for image halftoning using a human visual system. *SPSE's 43rd Annual Conference, RIT, Rochester*, (may 20-25), 1990.

[Stu75] P. Stucki. Comparison and optimization of computer-generated digital halftone pictures. *SID Digest of Technical Papers*, (6), 1975.

[Stu81] P. Stucki. Mecca - a multiple error correction computation algorithm for bi-level image hardcopy reproduction. *IBM Research Report RZ 1060, IBM Zurich Laboratory*, 1981.

[Tal52] W.H.F. Talbot. Improvements in the art of engraving. *Britisch Patent Specification*, (565), 19 oct. 1852.

[Uli87] R. Ulichney. Digital halftoning. *MIT Press, Cambridge, Mass.*, 1987.

[vdB90] P. van den Bulck. A two-dimensional filter model for error diffusion. *Deutsche Gesellschaft für angewandte Optik, Conference in Interlaken, Schweiz*, june, 1990.

[WN82] I.H. Witten and M. Neal. Using peano curves for bilevel display of continuous-tone images. *IEEE Comp. Graph. and Applic.*, may, 1982.

[WWB89] S. Weissbach, F. Wyrowski, and O. Bryngdahl. Digital phase holograms coding and quantization with an error diffusion concept. *Optics Communications*, 72(1,2):37–41, 1989.

[WWB90] S. Weissbach, F. Wyrowski, and O. Bryngdahl. Fehlerdiffusionsverfahren in der digitalen optik. *Deutsche Gesellschaft für angewandte Optik, Conference in Interlaken, Schweiz*, june, 1990.

[Wyr90] F. Wyrowski. Diffractive optical elements: iterative calculation of quantized, blazed phase structures. *Journal of the Optical Society of America*, 7(6):961–969, 1990.